Scheme 1. Synthesis of Optically Active 1,3-Dioxacycloalkanes

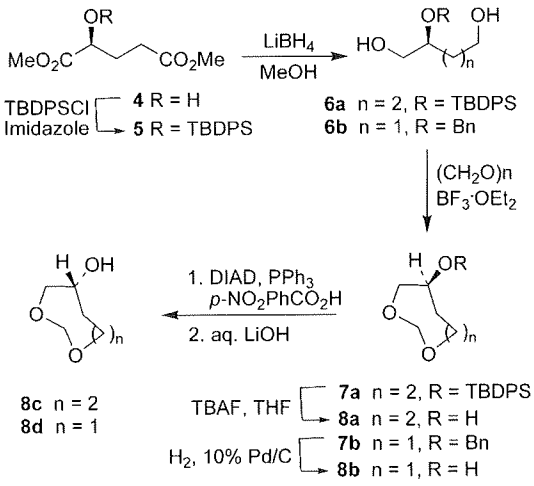

Scheme 2. Synthesis of Cyclic Ether **8e**

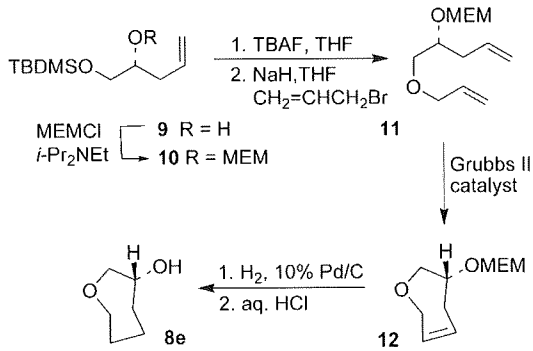

Scheme 3. Synthesis of Cyclic Ether **8f**

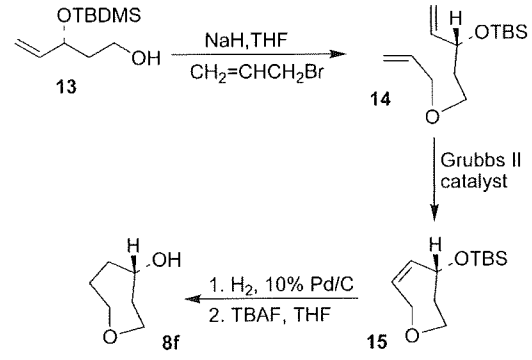

2) was protected as the corresponding methoxyethoxymethyl (MEM)-ether **10** in 90% yield using an excess of MEM-Cl in the presence of DIPEA in CH_2Cl_2.

Subsequent n-$Bu_4N^+F^-$-promoted deprotection of the TBDMS-group afforded the corresponding primary alcohol, which was treated with sodium hydride and alkylated with allyl bromide in the presence of a catalytic amount of n-$Bu_4N^+I^-$ to afford olefin **11** in 78% yield (2 steps). A 0.01 M solution of **11** in CH_2Cl_2 was then treated with a catalytic amount (5 mol%) of second generation Grubbs catalyst and heated to 45 °C to afford the cyclooxepane **12** in 94% yield. The double bond of **12** was finally reduced by catalytic hydrogenation using 10% Pd−C as the catalyst, and the MEM-ether was removed by acidic hydrolysis in a 1:1 THF/H_2O mixture to obtain the target alcohol **8e** in good overall yield.

For the synthesis of alcohol **8f** (Scheme 3), compound **13** was used as the starting material. It was in turn prepared following a described procedure starting from acrolein and *tert*-butylacetate.[23] Alkylation of the primary hydroxyl group of **13** with allyl bromide and n-$Bu_4N^+I^-$ using sodium hydride as the base furnished the ring closing metathesis precursor **14**. The cyclization reaction was performed by using second generation Grubbs catalyst (5 mol%) in CH_2Cl_2 and afforded olefin **15** in good yield. Subsequent hydrogenation of the double bond and n-$Bu_4N^+F^-$-mediated removal of TBDMS-ether finally afforded the target alcohol **8f**.

Scheme 4. Synthesis of Polyethers **8h−j**

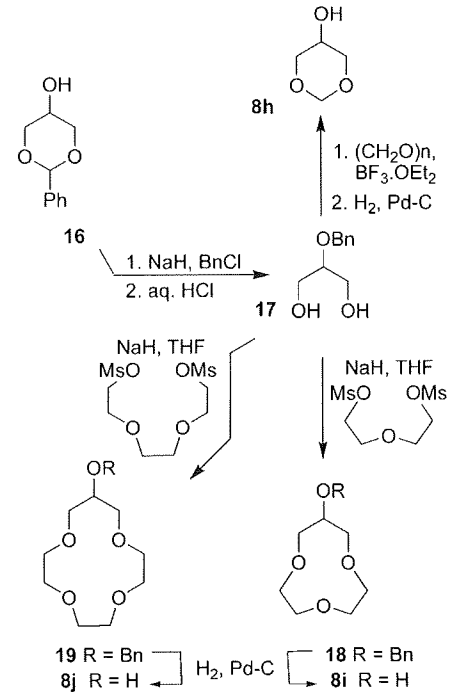

Alcohols **8h−j** required for the preparation of inhibitors **3h−j** were synthesized by starting from the common intermediate 2-benzyloxypropane-1,3-diol **17** as shown in Scheme 4. Compound **17** was prepared by alkylation of commercially available benzylidene acetal **16** with benzyl chloride in the presence of sodium hydride and a catalytic amount of n-$Bu_4N^+I^-$ in THF at 23 °C. The benzylidene group was subsequently removed by hydrolysis with 6 N HCl in a mixture (1:1) of THF and water to give 2-benzyloxy-1,3-propanediol **17** in quantitative yield. Treatment of **17** with paraformaldehyde and $BF_3 \cdot OEt_2$ as described above, followed by hydrogenolysis of the resulting *O*-benzylether afforded **8h** in 78% overall yield.

Treatment of diol **17** with an excess of sodium hydride in refluxing THF followed by addition of di(ethyleneglycol)dimesylate or tri(ethyleneglycol)dimesylate afforded macrocycles **18** and **19** in 19% and 29% yield, respectively. Dilution of the reaction mixture to assist the intramolecular cyclization reaction did not result in a significant improvement of the reaction yields. Given the poor enzymatic inhibitory activity observed for the corresponding final compounds **3i** and **3j**, no further attempts were made to improve the cyclization yield for the preparation of these 10- and 13-membered polyether rings. Compounds **18** and **19** were subsequently deprotected by hydrogenolysis to obtain alcohols **8i** and **8j**.

We planned to investigate the effect of heteroatom functionalities in the polyether rings. In this context, we prepared the compounds **8k**, **8l**, and **24** from known diols **20**[24] as shown in Scheme 5. Thus, exposure of **20** to paraformaldehyde in the presence of $BF_3 \cdot OEt_2$ furnished the corresponding cyclic

Scheme 5. Synthesis of Alcohols **8k,l** and **24**

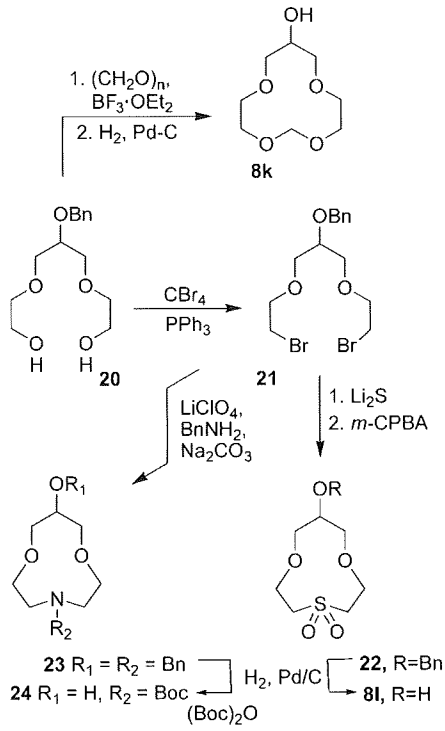

polyether product, which, upon hydrogenolysis, gave alcohol **8k**. Bromination of **20** using carbon tetrabromide and triphenylphosphine afforded dibromide **21**.[24] This dibromide was used for the synthesis of sulfone **8l** and protected amine **24**. Thus, compound **21** was reacted with one equivalent of benzylamine in refluxing MeCN in the presence of sodium carbonate, as reported by Calverley and Dale,[25] to provide **23** in 24% yield. Dimerization is the main side product in this reaction and one can reduce such dimerization by using an excess of $LiClO_4$.[26] Benzylamine **23** was hydrogenated over 10% Pd−C in the presence of di-*t*-butyl dicarbonate to provide *N*-Boc protected alcohol **24**. Sulfone **22** was obtained by cyclization of **21** with lithium sulfide, followed by oxidation of the corresponding sulfide with an excess of *m*-CPBA in CH_2Cl_2 at 23 °C. Benzyl derivative **22** was converted to **8l** by a catalytic hydrogenation over 10% Pd−C.

Scheme 6 depicts the conversion of various P2-ligands to the corresponding active carbonates for urethane formation. Accordingly, alcohols **8a−h,j−l** were reacted with *p*-nitrophenylchloroformate and *N*-methylmorpholine in THF at 23 °C to provide corresponding carbonates **25a−h,j−l** in 67−89% yields. Alcohol **8i** was converted to succinimidylcarbamate **25i** by treatment with *N,N′*-succinimidylcarbonate in the presence of Et_3N in MeCN in 37% isolated yield.

The synthesis of designed inhibitors **3a−l** is shown in Scheme 7. Methoxysulfonamide derivative **27** was prepared from commercially available epoxide **26** as described previously.[27] The Boc group in **27** was removed by exposure to a 30% solution of TFA in CH_2Cl_2 at 23 °C. The resulting amine **28** was reacted with the suitable mixed activated carbonates **25a−l** in THF at 23 °C for 2−4 days to furnish inhibitors **3a−l** in 36−89% yield.

The synthesis of inhibitor **3m** is shown in Scheme 8. Alcohol **24** was converted to active carbonate **29** as described above in Scheme 6. Reaction of **29** with amine **28** provided urethane **30** in good yield. Removal of Boc group of **30** by exposure to 30% TFA in CH_2Cl_2 furnished amine **31**. The resulting secondary

Scheme 6. Synthesis of Various Active Carbonates

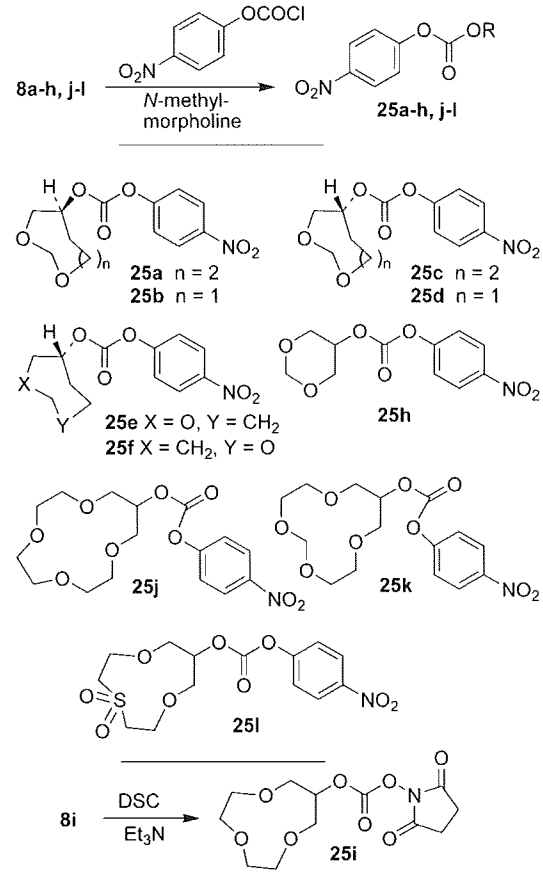

Scheme 7. Synthesis of Inhibitors **3a−l**

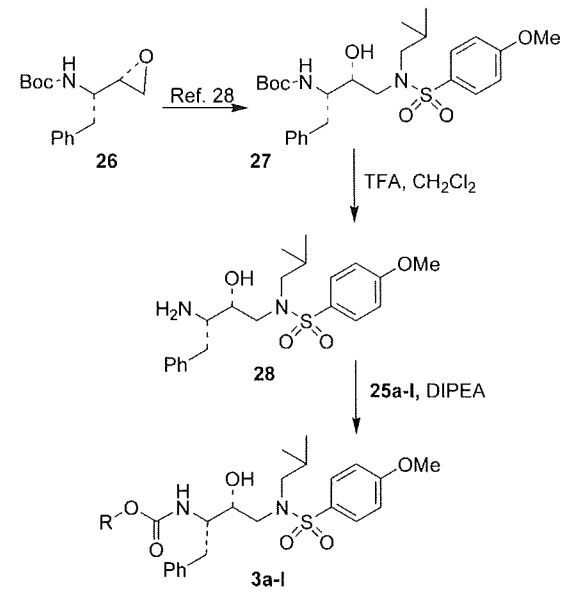

amine was subjected to a reductive amination reaction using 37% aqueous formaldehyde and sodium cyanoborohydride in 1% acetic acid in MeOH to furnish *N*-methyl derivative **3m** in 87% yield.

Results and Discussion

All inhibitors contain a (*R*)-hydroxyethylamine sulfonamide isostere with a *p*-methoxysulfonamide as the P2′-ligand and various designed cyclic ethers and polyethers as the P2-ligands.

Scheme 8. Synthesis of Inhibitor **3m**

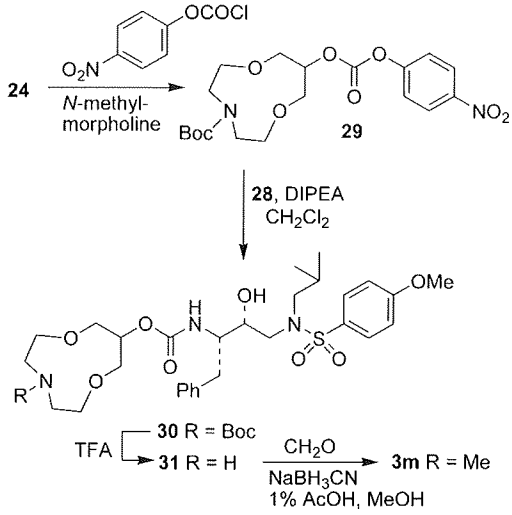

These inhibitors were first evaluated in an enzyme inhibitory assay utilizing a protocol described by Toth and Marshall.[28] Compounds that showed potent enzymatic K_i values were then further evaluated in an antiviral assay. The results are shown in Table 1. The K_i-values denote the mean values of at least four determinations.

As it can be seen, introduction of the 8-membered (*S*)- or (*R*)-1,3-dioxacyclooctan-5-yl urethanes as P2-ligands (inhibitors **3a** and **3c**) resulted in subnanomolar inhibitors. However, these inhibitors are significantly less potent than inhibitor **2** that contains the bis-THF ligand. Interestingly, incorporation of a (5*R*)-1,3-dioxacycloheptan-5-yl urethane as the P2-ligand resulted in the most potent inhibitor **3d** in this series with a K_i value of 26 pM. We speculated that the 7-membered 1,3-dioxepanyl-ligand with *R*-configuration may bind to residues in the S2-site similar to bis-THF ligand of inhibitor **2**. Inhibitor **3d** exhibited more than 6-fold potency increase relative to epimeric (5*S*)-1,3-dioxacycloheptan-5-yl urethane **3b**, suggesting an important role for the ring stereochemistry. Inhibitors **3e**−**g** were prepared to assess the role played by both oxygen atoms of **3d** on the binding mode of this latter compound. As shown in Table 1, a dramatic drop in enzymatic inhibitory activity was observed when the cycloheptanol was introduced as the P2-ligand (**3g**). Moreover, nearly 30-fold reduction in enzymatic inhibitory potency of both **3e** and **3f** with respect to **3d** clearly demonstrated that both oxygen atoms are crucial for the interaction with the enzyme at the S2-subsite. It appears that both oxygen atoms engage in strong hydrogen bonding, which equally contribute to the binding affinity for the enzyme. This result was further confirmed by the determination of the X-ray crystal structure of **3d**-bound HIV-1 protease.

Further reduction of the ring size of the P2-ligand resulted in the design of inhibitor **3h**, bearing a 6-membered 1,3-dioxan-5-yl urethane. This inhibitor also showed an impressive enzymatic K_i value of 41 pM. This result suggested that the 1,3-dioxane ring could be nicely accommodated by the S2-site. Furthermore, both oxygens may be involved in specific interactions with the amino acid residues in this region.

Subsequently, we tested compounds **3i**−**m**, presenting larger polyether rings, but all compounds showed K_i values in the high nM range (K_is ranging from 6.3 to 33 nM), proving that large rings could not be easily accommodated at the S2-site.

However, subtle differences in the activity among these compounds suggested that not only the ring size, but also the position of the oxygen atoms within the polyether structure, could be important for inhibitory activity. In fact, compound **3k**, presenting a 12-membered ring bearing a methylenedioxy unit instead of the ethylenedioxy of **3j**, exhibited 5-fold potency enhancement compared to inhibitor **3j**. It is also more than 2-fold more potent compared to **3i**, which contains a smaller 10-membered ring. Substitution of a ring oxygen in **3i** by a *N*-Me group provided inhibitor **3m** with no change in inhibitory activity. However, replacement of ring oxygen with a SO_2 moiety provided inhibitor **3l** with a 9-fold improvement in potency. The sulfone oxygens may be involved in specific interactions with the amino acid residues at the S2 site.

In MT-2 human T-lymphoid cells exposed to HIV-1_{LAI}, inhibitors **3d** and **3h** have shown antiviral IC_{50} values of 4.9 nM and 3.4 nM, respectively (Table 1). Consistent with its enzymatic potency, compound **3b** showed an antiviral activity of 30 nM in the same assay system, while compounds **3k**−**m** did not exhibit appreciable antiviral properties at doses up to 1 μM. We have examined two selected compounds, **3d** and **3h**, for their activity against HIV-1 using a human CD4+ T-cell line (MT-2 cells) and human peripheral blood mononuclear cells (PBMCs) as target cells. We employed two end points for the activity against HIV-1: (i) the inhibition of the HIV-1-elicited cytopathic effect for MT-2 cells and (ii) the inhibition of HIV-1 p24 production for PBMCs.[14a] As examined in MT-2 cells as target cells, the two compounds **3d** and **3h** exerted extremely potent antiviral activity against an X4-HIV-1 isolate (HIV-1_{LAI}) with IC_{50} values of 4.9 and 3.4 nM, respectively (Table 1). Such anti-HIV-1 potency was generally parallel to the potency in enzymatic inhibition of the compounds. We further examined the two compounds in PBMCs against a clinical wild-type X4-HIV-1 isolate (HIV-$1_{ERS104pre}$) along with various multidrug-resistant clinical X4- and R5-HIV-1 isolates (Table 2).[14] The activity of **3d** and **3h** against HIV-$1_{ERS104pre}$ was more potent or at least comparable as compared to those of currently available protease inhibitors, APV, IDV, and RTV. It is interesting to note that the values of **3d** were greater than those with MT-2 cells by factors of about 4. With regard to this difference, considering that **3d** was highly potent as examined in human T cells (MT-2 cells) but its activity was slightly less in PBMCs, it is possible that relatively higher concentrations of **3d** are required to suppress HIV-1 production in chronically infected macrophages.[42] Two currently available protease inhibitors (IDV and RTV) were not capable of efficiently suppressing the replication of most of the multidrug-resistant clinical isolates examined (HIV-1_{MDR-B}, HIV-1_{MDR-G}, HIV-1_{MDR-TM}, HIV-$1_{MDR-JSL}$, and HIV-1_{MDR-MM}) with IC_{50} values of >1.0 μM. Although the two selected compounds were also less potent against the multidrug-resistant clinical isolates examined, their IC_{50} values were quite low with 0.22−0.54 μM (Table 2). During testing of the anti-HIV-1 activity of compounds **3b**, **3d**, **3h**, and **3k**−**m**, we examined four concentrations (1, 0.1, 0.01, and 0.001 μM) in the antiretroviral assay, conducted on three independent occasions (each assay was performed in duplicate). As noted, no cytotoxicity was observed for any of the compounds examined. Thus, it was deemed that the CC_{50} values were greater than the highest concentration, 1 μM.

X-ray Crystallography. The mode of binding of the inhibitor was determined by analyzing the atomic resolution crystal structure of HIV-1 protease with **3d**. The crystal structure was solved and refined to an R factor of 14.9% at 1.00 Å resolution. The inhibitor binds with extensive interactions from P2 to P2′ with the protease atoms and, most notably, the favorable polar

Table 2. Antiviral Activity (IC_{50}) of Inhibitors **3d** and **3h** against Clinical HIV-1 Isolates in PBMC Cells (nM)

	IC_{50} (nM) values[a]					
virus	**3d**	**3h**	DRV	RTV	APV	IDV
ERS104pre(wild-type)	20	6	3.5	34	33	26
MDR/TM	220 (11)	64 (10)	4 (1)	>1000 (>29)	290 (9)	>1000 (>38)
MDR/MM	250 (13)	110 (5)	17 (5)	>1000 (>29)	300 (9)	>1000 (>38)
MDR/JSL	500 (25)	330 (55)	26 (7)	>1000 (>29)	430 (13)	>1000 (>38)
MDR/B	340 (17)	230 (38)	26 (7)	>1000 (>29)	320 (10)	>1000 (>38)
MDR/C	210 (11)	160 (27)	7 (2)	>1000 (>29)	230 (7)	>1000 (>38)
MDR/G	360 (18)	300 (50)	7 (2)	>1000 (>29)	340 (10)	290 (11)
MDR/A	20 (1)	13 (2)	3 (1)	>1000 (>29)	100 (3)	>1000 (>38)

[a] Amino acid substitutions identified in the protease-encoding region compared to the consensus type B sequence cited from the Los Alamos database include L63P in HIV-$1_{ERS104pre}$; L10I, K14R, L33I, M36I, M46I, F53I, K55R, I62V, L63P, A71V, G73S, V82A, L90M, and I93L in HIV-1_{MDR-B}; L10I, V11I, T12E, I15V, L19I, R41K, M46L, L63P, A71T, V82A, and L90 M in HIV-1_{MDR-G}; L10I, K14R, R41K, M46L, I54V, L63P, A71V, V82A, L90M, I93L in HIV-1_{MDR-TM}; L10I, L24I, I33F, E35D, M36I, N37S, M46L, I54V, R57K, I62V, L63P, A71V, G73S, and V82A in HIV-$1_{MDR-JSL}$; and L10I, K43T, M46L, I54V, L63P, A71V, V82A, L90M, and Q92K in HIV-1_{MDR-MM}. HIV-$1_{ERS104pre}$ served as a source of wild-type HIV-1.The IC_{50} values were determined by employing PHA-PBMC (phytohemaglutinin-activated peripheral blood mononuclear cells) as target cells and the inhibition of p24Gag protein production as the end point. All values were determined in triplicate. DRV (Darunavir), SQV (Saquinavir), APV (Amprenavir), IDV (Indinavir).

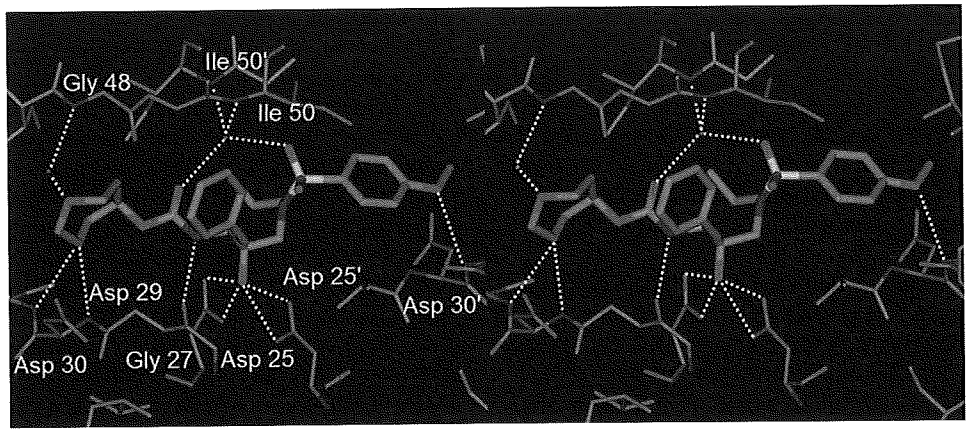

Figure 2. Stereoview of compound **3d** bound to the active site of wild-type HIV-1 protease.

interactions including hydrogen bonds, weaker C−H···O and C−H···π interactions, as shown in Figure 2. The central hydroxyl group forms hydrogen bonds to the side chain carboxylate oxygen atoms of the catalytic Asp25 and Asp25′ residues. The inhibitor hydrogen bonds with protease main chain atoms of the amides of Asp29 and Asp30, the carbonyl oxygen of Gly 27, and the water-mediated interactions with the amides of Ile50 and 50′, which is conserved in the majority of protease complexes with inhibitors[29] and substrate analogues.[30] Inhibitor **3d** has retained the water-mediated interaction with the π system of the P2′ aromatic ring, which was observed for darunavir (**1**) and GRL-98065.[31] The P2′ methoxy group forms a hydrogen bond with the amide of Asp30′. Interestingly, the P2 group forms a water-mediated interaction with the amide of Gly48, similar to the interactions described for several peptide substrate analogues.[30]

Conclusions. In summary, a series of novel and highly potent HIV-1 protease inhibitors were designed, synthesized, and evaluated. The inhibitors incorporate a variety of flexible cyclic ethers/polyethers as the P2-ligand. Inhibitors containing small size 1,3-dioxacycloakanes have shown potent inhibitory properties. In particular, inhibitors **3d** and **3h** have shown remarkable enzyme inhibitory and antiviral potency. Inhibitors incorporating medium-size cyclic polyethers or polyethers containing a sulfone or amine functionality were significantly less potent in antiviral assays. For inhibitor **3d**, we have carried out an optically active synthesis of (*R*)-1,3-dioxepan-5-ol using (*S*)-malic acid as the starting material. Syntheses of various cyclic ethers/polyethers were developed albeit in moderate yields. Inhibitor **3d** has shown excellent activity against multi-PI-resistant variants compared to other FDA approved inhibitors. A protein−ligand X-ray structure of **3d**-bound HIV-1 protease was determined at 1.0 Å resolution. One of the oxygens of the 1,3-dioxepane ligand is involved in hydrogen bonding with Asp29 and Asp30 NH's. The other oxygen is involved in a unique interaction with Gly-48 NH through a water molecule. One goal of our inhibitor design strategy is to combat drug-resistant HIV. The design of inhibitor using the concept of maximizing "backbone binding" has led to the development of PIs characterized by high potency against both wild-type and multidrug-resistant HIV-1 strains. Further design of inhibitors utilizing this molecular insight is in progress.

Experimental Section

General. All moisture sensitive reactions were carried out under nitrogen or argon atmosphere. Anhydrous solvents were obtained as follows: THF, diethyl ether and benzene, distilled from sodium and benzophenone; dichloromethane, pyridine, triethylamine, and diisopropylethylamine, distilled from CaH_2. All other solvents were HPLC grade. Column chromatography was performed with Whatman 240−400 mesh silica gel under low pressure of 5−10 psi. TLC was carried out with E. Merck silica gel 60-F-254 plates. ^1H and ^{13}C NMR spectra were recorded on Varian Mercury 300 and Bruker Avance 400 and 500 spectrometers. Optical rotations were measured using a Perkin-Elmer 341 polarimeter.

(*S*)-2-(*tert*-Butyldiphenylsilyloxy)pentadioic Acid Dimethyl Ester (5). A mixture of (2*S*)-hydroxypentadioic acid dimethyl ester **4**[18] (0.39 g, 2.2 mmol), imidazole (0.45 g, 6.6 mmol), and *tert*-butyldiphenylsilyl chloride (1.2 mL, 4.4 mmol) in dry DMF (4 mL) was stirred at 23 °C for 4 h. Subsequently, the reaction mixture was poured into water and the aqueous phase was extracted with Et_2O, the organic extracts were washed with 1 N HCl and brine, dried (Na_2SO_4), and the solvent was removed. The residue was

purified by flash-chromatography (1:10 EtOAc/hex) to furnish 0.89 g (90%) of **5** as a colorless oil: $[\alpha]_D^{20}$ −21.1 (*c* 9.0, $CHCl_3$). ^1H NMR ($CDCl_3$) δ 7.69−7.62 (m, 4H), 7.46−7.33 (m, 6H), 4.31 (t, J = 5.4 Hz, 1H), 3.64 (s, 3H), 3.45 (s, 3H), 2.57−2.34 (m, 2H), 2.14−2.04 (m, 2H), 1.11 (s, 9H). ^{13}C NMR ($CDCl_3$) δ 173.4, 172.9, 135.9, 135.7, 133.0, 132.9, 129.9, 129.8, 127.7, 127.5, 71.4, 51.6, 51.5, 29.9, 28.9, 26.9, 19.4.

(*S*)-2-(*tert*-Butyldiphenylsilyloxy)pentan-1,5-diol (6a). Compound **5** (0.8 g, 1.8 mmol) was dissolved in dry Et_2O (8.5 mL) and the solution was cooled to 0 °C, afterward lithium borohydride (0.12 g, 5.4 mmol) and dry methanol (0.22 mL, 5.4 mmol) were sequentially added. The resulting suspension was stirred at 23 °C for 24 h, then a few drops of 6 N HCl were added and the salts were filtered off. The filtrate was concentrated under reduced pressure and the residue was purified by flash-chromatography (1:1 EtOAc/hex) to furnish 0.61 g (93%) of **6a** as a colorless oil: $[\alpha]_D^{20}$ −15.6 (*c* 3.1, $CHCl_3$). ^1H NMR ($CDCl_3$) δ 7.70−7.65 (m, 4H), 7.44−7.32 (m, 6H), 3.82−3.77 (m, 1H), 3.53−3.48 (m, 2H), 3.45−3.41 (m, 2H), 1.65−1.47 (m, 4H), 1.05 (s, 9H). ^{13}C NMR ($CDCl_3$) δ 135.9, 135.7, 133.8, 133.7, 130.1, 129.8, 127.7, 127.6, 73.6, 65.7, 62.7, 29.7, 28.0, 27.0, 19.3.

(*S*)-1-(*tert*-Butyldiphenylsilyloxy)-3,5-dioxacyclooctane (7a). To a mixture of **6a** (0.55 g, 1.5 mmol) and paraformaldehyde (46 mg, 1.5 mmol) in EtOAc (30 mL), boron trifluoride etherate (195 μL, 1.5 mmol) was added and the resulting mixture was stirred at 23 °C for 4 h. The organic phase was washed with a saturated solution of $NaHCO_3$, dried (Na_2SO_4), and the solvent was removed. The residue was purified by flash-chromatography (1:4 EtOAc/hex) to afford 0.29 g (51%) of **7a** as a colorless oil: $[\alpha]_D^{20}$ −8.7 (*c* 1.9, $CHCl_3$). ^1H NMR ($CDCl_3$) δ 7.67−7.63 (m, 4H), 7.45−7.34 (m, 6H), 4.69 (d, J = 6.2 Hz, 1H), 4.45 (d, J = 6.2 Hz, 1H), 4.03−3.95 (m, 1H), 3.70−3.61 (m, 1H), 3.59−3.48 (m, 3H), 1.93−1.80 (m, 1H), 1.77−1.61 (m, 2H), 1.47−1.34 (m, 1H), 1.12 (s, 9H). ^{13}C NMR ($CDCl_3$) δ 135.7, 134.2, 129.5, 127.5, 95.6, 72.2, 71.9, 69.0, 33.2, 27.0, 26.7, 19.2.

(*S*)-*O*-Benzyl-3,5-dioxacycloheptan-1-ol (7b). Compound **6b**[20] (50 mg, 0.26 mmol) was reacted as described for compound **6a** to afford 44 mg (82%) of **7b** after chromatographic purification (1:9 EtOAc/hex): $[\alpha]_D^{20}$ +64.6 (*c* 1.2, $CHCl_3$). ^1H NMR ($CDCl_3$) δ 7.35−7.26 (m, 5H), 4.81−4.77 (m, 2H), 4.58 (s, 2H), 3.95−3.73 (m, 3H), 3.73−3.62 (m, 2H), 1.98−1.91 (m, 2H). ^{13}C NMR ($CDCl_3$) δ 138.3, 128.3, 127.5, 126.2, 94.9, 75.8, 70.7, 68.8, 62.6, 35.0.

(*S*)-3,5-Dioxacyclooctan-1-ol (8a). Compound **7a** (0.27 g, 0.74 mmol) was dissolved in dry THF (5 mL) and TBAF (1.0 M solution in THF, 0.81 mL, 0.81 mmol) was added. The resulting mixture was stirred at 23 °C overnight, afterward a saturated solution of $NaHCO_3$ was added, the solvent was removed, and the aqueous phase was extracted with EtOAc. The organic extracts were dried and evaporated and the residue was purified by flash-chromatography (EtOAc) to afford 76 mg (77%) of **8a** as a colorless oil: $[\alpha]_D^{20}$ −12.6 (*c* 1.6, $CHCl_3$). ^1H NMR ($CDCl_3$) δ 4.65 (d, J = 6.0 Hz, 1H), 4.57 (d, J = 6.0 Hz, 1H), 4.92−3.81 (m, 2H), 3.75−3.60 (m, 2H), 3.55 (dd, J = 3.4, 12.1 Hz, 1H), 2.96 (bs, 1H), 1.95−1.69 (m, 3H), 1.65−1.53 (m, 1H). ^{13}C NMR ($CDCl_3$) δ 94.9, 73.7, 69.3, 68.2, 30.2, 24.7.

(*S*)-3,5-Dioxacycloheptan-1-ol (8b). To a solution of **7b** (38 mg, 0.18 mmol) in EtOAc (3 mL), 10% Pd/C was added and the resulting suspension was stirred at 23 °C under a hydrogen atmosphere. After 12 h, the catalyst was filtered off, the filtrate was evaporated in vacuo, and the residue (19 mg, 91%) was used in the next step without further purification: $[\alpha]_D^{20}$ +12.9 (*c* 0.9, $CHCl_3$). ^1H NMR ($CDCl_3$) δ 4.78−4.74 (m 2H), 3.93−3.91 (m, 1H), 3.81−3.75 (m, 4H), 2.51 (bs, 1H), 1.93−1.83 (m, 2H). ^{13}C NMR ($CDCl_3$) δ 94.4, 69.5, 68.4, 62.3, 37.8.

(*R*)-3,5-Dioxacyclooctan-1-ol (8c). To a mixture of (*S*)-**8a** (46 mg, 0.35 mmol), *p*-nitrobenzoic acid (86 mg, 0.52 mmol), and triphenylphosphine (181 mg, 0.69 mmol), diisopropylazodicarboxylate (135 μL, 0.69 mmol) was added dropwise and the resulting mixture was stirred at 23 °C overnight. The solvent was removed under reduced pressure, and the residue was purified by flash-chromatography (1:3 EtOAc/hex). The resulting ester was dissolved in a 3:2:1 mixture of THF, methanol, and water (4 mL) and $LiOH \cdot H_2O$ (72 mg, 1.7 mmol) was added. The yellow mixture was stirred at 23 °C overnight and then the solvent was removed in vacuo, the residue was diluted with water, and the aqueous phase was extracted with ether. The organic extracts were dried (Na_2SO_4) and the solvent evaporated. Purification of the residue by flash-chromatography (EtOAc) afforded 20 mg (44%) of (*R*)-**8c** as a colorless liquid. $[\alpha]_D^{20}$ +12.1 (*c* 1.4, $CHCl_3$). ^1H and ^{13}C NMR are consistent with those reported for the (*S*)-enantiomer **8a**.

(*R*)-3,5-Dioxacycloheptan-1-ol (8d). The title compound was obtained from **8b** as described for (*S*)-**8c** in 73% yield. Flash-chromatography was performed using a 1:1 mixture of EtOAc and $CHCl_3$ as the eluant: $[\alpha]_D^{20}$ −12.6 (*c* 1.3, $CHCl_3$). ^1H and ^{13}C NMR are consistent with those reported for the (*S*)-enantiomer **8b**.

(*R*)-1-(*tert*-Butyldimethylsilyloxy)-2-[(2-methoxyethoxy) methoxy]pent-4-ene (10). To a mixture of **9** (350 mg, 1.6 mmol) and diisopropylethylamine (1.2 mL, 7.2 mmol) in CH_2Cl_2 (8 mL), cooled to 0 °C, MEM-Cl (550 μL, 4.8 mmol) was added and the resulting mixture was stirred at 23 °C for 56 h. The organic phase was washed with 0.1 N HCl, brine and dried (Na_2SO_4). The solvent was removed and the residue was purified by flash-chromatography (1:10 EtOAc/hex) to afford 440 mg (90%) of **10** as a colorless oil: $[\alpha]_D^{20}$ +12.0 (*c* 1.1, $CHCl_3$). ^1H NMR ($CDCl_3$) δ 5.88−5.74 (m, 1H), 5.11−5.01 (m, 2H), 4.82 (d, J = 6.9 Hz, 1H), 4.74 (d, J = 6.9 Hz, 1H), 3.76−3.63 (m, 3H), 3.60−3.51 (m, 4H), 3.37 (s, 3H), 2.38−2.19 (m, 2H), 0.86 (s, 9H), 0.02 (s, 6H). ^{13}C NMR ($CDCl_3$) δ 134.6, 117.0, 94.8, 77.4, 71.6, 66.7, 65.0, 58.9, 36.0, 25.7, 18.2, −5.5.

(*R*)-1-Allyloxy-2-[(2-methoxyethoxy)methoxy]pent-4-ene (11). A mixture of **10** (440 mg, 1.4 mmol) and TBAF (1.0 M solution in THF, 4.7 mL, 4.7 mmol) in THF (3 mL) was stirred at 23 °C for 3 h, afterward a saturated solution of $NaHCO_3$ was added, the solvent was removed, and the aqueous phase was extracted with $CHCl_3$. The organic extracts were dried (Na_2SO_4), and the solvent was removed. The residue was purified by flash-chromatography to afford 237 mg (87%) of (*R*)-2-[(2-methoxyethoxy)methoxy]pent-4-en-1-ol as a colorless oil: $[\alpha]_D^{20}$ −55.0 (*c* 1.3, $CHCl_3$). ^1H NMR ($CDCl_3$) δ 5.85−5.71 (m, 1H), 5.11−5.02 (m, 2H), 4.81 (d, J = 7.5 Hz, 1H), 4.75 (d, J = 7.5 Hz, 1H), 3.87−3.80 (m, 1H), 3.71−3.61 (m, 3H), 3.59−3.46 (m, 3H), 3.37 (s, 3H), 3.22 (bs, 1H), 2.36−2.19 (m, 2H). ^{13}C NMR ($CDCl_3$) δ 134.1, 117.3, 95.4, 81.0, 71.5, 67.3, 64.8, 58.9, 36.2. To a mixture of the above compound (240 mg, 1.25 mmol), allyl bromide (225 μL, 1.9 mmol) and a catalytic amount of TBAI in THF (12 mL), at 0 °C, sodium hydride (60% dispersion in oil, 102 mg, 2.5 mmol) was added in small portions. After 30 min, the reaction mixture was allowed to warm to 23 °C and was stirred at the same temperature for 18 h. Subsequently, the reaction was quenched with a saturated solution of NH_4Cl, the organic solvent was removed, and the aqueous phase was extracted with $CHCl_3$. The organic extracts were dried (Na_2SO_4), and the solvent was evaporated. The residue was purified by flash-chromatography (10:1 $CHCl_3$/EtOAc) to afford 229 mg (80%) of **11** as a colorless oil. $[\alpha]_D^{20}$ −5.2 (*c* 3.1, $CHCl_3$). ^1H NMR ($CDCl_3$) δ 5.87−5.79 (m, 2H), 5.34 (dd, J = 1.3, 19.1 Hz, 1H), 5.16−5.03 (m, 3H), 4.81 (d, J = 7.0 Hz, 1H), 4.77 (d, J = 7.0 Hz, 1H), 3.98−3.97 (m, 2H), 3.84−3.81 (m, 1H), 3.72 (t, J = 5.0 Hz, 2H), 3.54 (t, J = 5.0 Hz, 2H), 3.46−3.44 (m, 2H), 3.38 (s, 3H), 2.35−2.31 (m, 2H). ^{13}C NMR ($CDCl_3$) δ 134.6, 134.3, 117.3, 116.7, 94.6, 75.3, 72.1, 71.9, 71.6, 66.7, 58.9, 36.3.

(*R,Z*)-3-[(2-Methoxyethoxy)methoxy]-2,3,4,7-tetrahydrooxepine (12). A mixture of **11** (100 mg, 0.43 mmol) and second generation Grubbs catalyst (18 mg, 0.02 mmol) in CH_2Cl_2 (10 mL) was heated to 45 °C for 1 h. After this time, the solvent was removed and the residue was purified by flash-chromatography (5:1 $CHCl_3$/EtOAc) to afford 83 mg (94%) of **12** as a colorless oil: ^1H NMR ($CDCl_3$) δ 5.87−5.66 (m, 2H), 4.77−4.18 (m, 2H), 4.18−4.14 (m, 2H), 4.01−3.89 (m, 2H), 3.75−3.68 (m, 3H), 3.56−3.53 (m, 2H), 3.38 (s, 3H), 2.54−2.51 (m, 2H). ^{13}C NMR ($CDCl_3$) δ 130.6, 125.9, 94.3, 75.6, 75.1, 71.6, 70.3, 66.8, 58.9, 31.8.

(*R*)-Oxepan-3-ol (8e). A mixture of **12** (90 mg, 0.44 mmol) and a catalytic amount of 10% Pd/C in EtOAc (3 mL) was stirred at 23 °C under a hydrogen atmosphere for 3 h. After this time, the catalyst was filtered off through a pad of celite and the filtrate was concentrated under reduced pressure to afford (*R*)-3-[(2-methoxyethoxy)methoxy]oxepane (83 mg, 92%) as a colorless oil. ^{1}H NMR ($CDCl_3$) δ 4.70 (d, J = 7.2 Hz, 1H), 4.67 (d, J = 7.2 Hz, 1H), 3.83−3.58 (m, 7H), 3.50 (t, J = 4.6 Hz, 2H), 3.34 (s, 3H), 1.72−1.67 (m, 1H), 1.46−1.44 (m, 4H), 1.22−1.19 (m, 1H). ^{13}C NMR ($CDCl_3$) δ 93.9, 76.5, 73.7, 71.8, 71.6, 66.7, 58.8, 32.6, 30.7, 20.9. A mixture of the above compound (50 mg, 0.24 mmol) and 6 N HCl (0.5 mL) in THF (2 mL) was stirred at 23 °C for 16 h. The solvent was removed, and the aqueous phase was extracted with $CHCl_3$. The organic extracts were washed with a saturated solution of $NaHCO_3$, dried (Na_2SO_4), and the solvent was removed. The residue was purified by flash-chromatography (1:4 EtOAc/$CHCl_3$) to afford **8e** (24 mg, 84%) as a colorless oil: $[\alpha]_D^{20}$ −4.2 (*c* 0.8, $CHCl_3$). ^{1}H NMR ($CDCl_3$) δ 3.87−3.85 (m, 1H), 3.76−3.62 (m, 4H), 2.37 (bs, 1H), 1.78−1.65 (m, 5H), 1.54−1.52 (m, 1H). ^{13}C NMR ($CDCl_3$) δ 73.2, 70.7, 70.4, 36.4, 30.0, 20.2.

(*R*)-3-(*tert*-Butyldimethylsilyloxy)-5-(allyloxy)pent-1-ene (14). A mixture of **13** (50 mg, 0.23 mmol), allyl bromide (30 μL, 0.35 mmol), and a catalytic amount of TBAI was cooled to 0 °C and sodium hydride (60% in mineral oil, 11 mg, 0.28 mmol) was added. The resulting mixture was allowed to warm to 23 °C and stirred for 18 h. The reaction was quenched by adding a saturated solution of NH_4Cl, the solvent was removed, and the aqueous phase was extracted with $CHCl_3$. The organic extracts were dried (Na_2SO_4), and the solvent was removed. The residue was purified by flash-chromatography (1:20 EtOAc/hex) to afford 57 mg (97%) of **14** as a colorless oil. ^{1}H NMR ($CDCl_3$) δ 5.96−5.87 (m, 1H), 5.85−5.78 (m, 1H), 5.29−5.24 (m, 1H), 5.19−5.13 (m, 2H), 5.04−5.00 (m, 1H), 4.31−4.26 (m, 1H), 3.96−3.94 (m, 2H), 3.55−3.42 (m, 2H), 1.84−1.67 (m, 2H), 0.90 (s, 9H), 0.06 (s, 3H), 0.02 (s, 3H). ^{13}C NMR ($CDCl_3$) δ 141.5, 134.9, 116.6, 113.6, 71.8, 70.6, 66.5, 38.0, 25.8, 18.1, −4.5, −5.1.

(*R,Z*)-4-(*tert*-Butyldimethysilyloxy)-2,3,4,7-tetrahydrooxepine (15). The title compound was obtained from **14** as described for **12** in 80% yield. Flash-chromatography was performed using a 1:10 mixture of EtOAc and hex as the eluant. ^{1}H NMR ($CDCl_3$) δ 5.79−5.75 (m, 1H), 5.63−5.60 (m, 1H), 4.64−4.62 (m, 1H), 4.14−4.12 (m, 2H), 3.91−3.85 (m, 1H), 3.80−3.74 (m, 1H), 2.11−2.05 (m, 1H), 1.96−1.91 (m, 1H), 0.90 (s, 9H), 0.08 (s, 3H), 0.07 (s, 3H). ^{13}C NMR ($CDCl_3$) δ 138.4, 127.8, 69.9, 68.2, 67.4, 38.8, 25.8, 18.3, −4.8.

(*S*)-Oxepan-4-ol (8f). Hydrogenolysis of **15** was carried out as described for **8e** to afford (*S*)-4-(*tert*-butyldimethylsilyloxy)oxepane in 95% yield as a colorless oil. ^{1}H NMR ($CDCl_3$) δ 4.03−3.96 (m, 1H), 3.79−3.57 (m, 4H), 1.98−1.69 (m, 5H), 1.64−1.51 (m, 1H), 0.88 (s, 9H), 0.044 (s, 3H), 0.038 (s, 3H). ^{13}C NMR ($CDCl_3$) δ 70.2, 69.4, 64.2, 40.1, 34.5, 25.7, 23.7, 18.0, −4.9. Deprotection of the above compound was performed as described for compound **11** and afforded the title compound in 75% yield as a colorless oil. ^{1}H NMR ($CDCl_3$) δ 4.03−3.98 (m, 1H), 3.82−3.59 (m, 4H), 2.02−1.98 (m, 1H), 1.89−1.80 (m, 4H), 1.66−1.64 (m, 1H). ^{13}C NMR ($CDCl_3$) δ 70.5, 69.6, 64.7, 38.9, 34.9, 24.3.

2-(Benzyloxy)propane-1,3-diol (17). To a solution of **16** (2.5 g, 13.8 mmol) in dry THF (20 mL), cooled to 0 °C, NaH (60% in mineral oil, 0.56 g, 14 mmol) was added portionwise. After 30 min, tetra-*n*-butylammonium iodide (51 mg, 0.14 mmol) and a solution of benzyl bromide (1.65 mL, 13.9 mmol) in THF (5 mL) were added. The reaction mixture was stirred at 23 °C for 3 h; afterward, it was poured into ice. The organic solvent was removed, and the aqueous phase was extracted with $CHCl_3$. The organic extracts were dried (Na_2SO_4), and the solvent was removed. The crude 5-(benzyloxy)-2-phenyl-1,3-dioxane thus obtained was dissolved in a 1:1 mixture of THF and H_2O (60 mL), and to the resulting solution, 6 N HCl was slowly added. After stirring at 23 °C, the reaction mixture was brought to pH 8 by addition of a saturated solution of $NaHCO_3$, the solvent was removed, and the aqueous phase was extracted with diethyl ether. The organic extracts were dried and evaporated, and the residue was purified by flash-column chromatography (2:1 EtOAc/hex) to afford the title compound as a colorless oil in quantitative yield. Physical and spectroscopic data are consistent with those reported in the literature.[32]

1,3-Dioxan-5-ol (8h). To a mixture of **17** (100 mg, 0.55 mmol) and paraformaldehyde (17 mg, 0.55 mmol) in EtOAc (10 mL), boron trifluoride etherate (70 μL, 0.55 mmol) was added and the reaction mixture was stirred at 23 °C for 4 h. The organic phase was washed with a saturated solution of $NaHCO_3$, dried, and the solvent was removed. The residue was purified by flash-chromatography eluting with a 1:4 mixture of EtOAc and hexanes to afford 84 mg (78%) of *O*-benzyl-1,3-dioxan-5-ol as a colorless oil. The above compound was dissolved in EtOAc (3 mL), Pd/C was added, and the resulting suspension was stirred at rt under a hydrogen atmosphere. After 12 h, the catalyst was filtered off, the filtrate was evaporated in vacuo, and the residue (39 mg, 100%) was used in the next step without further purification: ^{1}H NMR ($CDCl_3$) δ 4.93 (d, J = 6.3 Hz, 1H), 4.76 (d, J = 6.3 Hz, 1H), 3.94−3.84 (m, 4H), 3.64−3.61 (m, 1H), 2.78 (bs, 1H). ^{13}C NMR ($CDCl_3$) δ 94.0, 71.7, 64.1.

***O*-Benzyl-3,6,9-trioxacyclodecan-1-ol (18).** To a refluxing suspension of sodium hydride (60% in mineral oil, prewashed with hexane, 84 mg, 2.1 mmol) in dry THF (5 mL), a solution of **17** (182 mg, 1.0 mmol) and di(ethyleneglycol)dimethanesulfonate (260 mg, 1.0 mmol) in dry THF (5 mL) was added dropwise. The resulting mixture was heated under reflux for 20 h and afterward was cooled to 23 °C and H_2O (2 mL) was added. The solvent was removed, and the aqueous phase was extracted with $CHCl_3$. The organic extracts were washed several times with water, dried (Na_2SO_4), and evaporated. The residue was purified by flash-chromatography (2:3 CH_2Cl_2/EtOAc) to afford 49 mg (19%) of **18** as a colorless oil. ^{1}H NMR ($CDCl_3$) δ 7.36−7.26 (m, 5H), 4.66 (s, 2H), 3.75−3.57 (m, 13H). MS (ESI) *m/z* 275 $[M + Na]^+$.

***O*-Benzyl-3,6,9,12-tetraoxacyclotridecan-1-ol (19).** Compound **19** was obtained as described for **18** starting from **17** and tri(ethyleneglycol)dimethanesulfonate in 29% yield. ^{1}H NMR ($CDCl_3$) δ 7.39−7.26 (m, 5H), 4.72 (s, 2H), 3.83−3.58 (m, 17 H). MS (ESI) *m/z* 319 $[M + Na]^+$.

3,6,9-Trioxacyclodecan-1-ol (8i). A mixture of **18** (34 mg, 0.13 mmol) and a catalytic amount of 10% Pd/C in methanol (2 mL) was stirred at 23 °C under a hydrogen atmosphere. After 18 h, the catalyst was filtered off and the filtrate was evaporated to afford 22 mg (99%) of **8i** as a colorless oil. ^{1}H NMR ($CDCl_3$) δ 3.74−3.53 (m, 13H), 2.73 (bs, 1H).

3,6,9,12-Tetraoxacyclotridecan-1-ol (8j). Starting from **19**, compound **8j** was obtained as described for **8i** in quantitative yield: ^{1}H NMR ($CDCl_3$) δ 3.81−3.60 (m, 17 H), 2.95 (bs, 1H).

3,6,8,11-Tetraoxa-1-cyclododecanol (8k). To a mixture of **20**[24] (78 mg, 0.29 mmol) and paraformaldehyde (8.7 mg, 0.29 mmol) in EtOAc (4 mL), boron trifluoride etherate (37 μL, 0.29 mmol) was added and the resulting mixture was stirred at 23 °C for 2 h. Subsequently, a saturated solution of $NaHCO_3$ was added and the aqueous phase was extracted with EtOAc. The combined organic extracts were dried (Na_2SO_4), and the solvent was removed in vacuo. The residue was purified by flash-chromatography to afford 31 mg (37%) of *O*-benzyl-3,6,8,11-tetraoxacyclododecan-1-ol as a colorless oil. ^{1}H NMR ($CDCl_3$) δ 7.35−7.27 (m, 5H), 4.67 (s, 2H), 3.88 (s, 2H), 3.86−3.81 (m, 2H), 3.77−3.61 (m, 11H). ^{13}C NMR ($CDCl_3$) δ 133.6, 128.3, 127.7, 126.2, 94.6, 75.8, 71.5, 69.6, 65.3, 64.6. MS (ESI) *m/z* 305 $[M + Na]^+$. A mixture of the above compound and a catalytic amount of 10% Pd/C in EtOAc (2 mL) was stirred at 23 °C under a hydrogen atmosphere. After 18 h, the catalyst was filtered off and the filtrate was evaporated to afford 21 mg (99%) of **8k** as a colorless oil. ^{1}H NMR ($CDCl_3$) δ 4.67 (s, 2H), 3.85−3.63 (m, 11H), 3.54 (dd, J = 6.4, 8.2 Hz, 2H), 2.22 (d, J = 8.7 Hz, 1H).

***O*-Benzyl-3,9-dioxa-6-thiacyclodecan-1-ol 6,6-dioxide (22).** A solution of lithium sulfide (11 mg, 0.23 mmol) in water (0.3 mL) was added dropwise within 30 min to a solution of **21**[24] (60 mg, 0.15 mmol) in refluxing ethanol (15 mL). The resulting mixture

was heated under reflux for 3 h and then was cooled to 23 °C. The solvent was removed and the aqueous phase was extracted with $CHCl_3$. The organic extracts were dried (Na_2SO_4), and the solvent was removed. Flash-chromatography of the residue (1:4 EtOAc/hexanes) afforded 16 mg (38%) of *O*-benzyl-3,9-dioxa-6-thiacyclodecan-1-ol as a colorless oil. ^{1}H NMR ($CDCl_3$) δ 7.36−7.27 (m, 5H), 4.59 (s, 2H), 3.90−3.85 (m, 2H), 3.82−3.48 (m, 7H), 2.91−2.74 (m, 4H). ^{13}C NMR ($CDCl_3$) δ 133.5, 128.3, 127.7, 126.0, 75.9, 71.9, 71.6, 68.0, 33.4. MS (ESI) *m/z* 291 $[M + Na]^+$, 286 $[M + H + NH_3]^+$, 269 $[M + H]^+$. To a solution of the above compound (11 mg, 0.040 mmol) in CH_2Cl_2 (2 mL), cooled to 0 °C, *m*-chloroperbenzoic acid (77%, 22 mg, 0.09 mmol) was added in small portions. After 18 h, a 1% solution of sodium bisulfite was added, the layers were separated, and the organic phase was washed with a saturated solution of $NaHCO_3$. The organic extracts were dried (Na_2SO_4) and evaporated. The residue was purified by flash-chromatography (1:4 EtOAc/$CHCl_3$) to afford 11 mg (93%) of **22** as a brown oil. ^{1}H NMR ($CDCl_3$) δ 7.37−7.29 (m, 5H), 4.57 (s, 2H), 4.01−3.96 (m, 4H), 3.77−3.72 (m, 1H), 3.66−3.60 (m, 4H), 3.40−3.38 (m, 2H), 3.34−3.23 (m, 2H). ^{13}C NMR ($CDCl_3$) δ 133.4, 128.4, 127.9, 127.7, 74.7, 71.8, 66.4, 64.6, 52.4.

3,9-Dioxa-6-thiacyclodecan-1-ol-6,6-dioxide (8l). A mixture of **22** (25 mg, 0.083 mmol) and a catalytic amount of 10% Pd/C in EtOAc (3 mL) was stirred at 23 °C under a hydrogen atmosphere. After 48 h, the catalyst was filtered off and the filtrate was evaporated to afford 16 mg (92%) of **8l** as a colorless oil. ^{1}H NMR ($CDCl_3$) δ 4.08−3.95 (m, 4H), 3.67 (dd, J = 4.2, 9.9 Hz, 2H), 3.61−3.59 (m, 1H), 3.51 (dd, J = 5.7, 9.9 Hz, 2H), 3.38−3.23 (m, 4H). ^{13}C NMR ($CDCl_3$) δ 69.0, 68.3, 64.5, 52.6.

***O*,6-Dibenzyl-3,9-dioxa-6-azocyclodecan-1-ol (23).** A mixture of **21**[24] (150 mg, 0.37 mmol), benzylamine (41 μL, 0.37 mmol), lithium perchlorate (340 mg, 3.7 mmol), and sodium carbonate (200 mg, 1.9 mmol) in acetonitrile (7.5 mL) was heated under reflux for 48 h. After cooling to 23 °C, the solvent was removed, the residue was suspended in $CHCl_3$, and the organic phase was washed with water and dried (Na_2SO_4). Flash-chromatography of the residue (2:1 EtOAc/$CHCl_3$) afforded 31 mg (24%) of **23** as a colorless oil. ^{1}H NMR ($CDCl_3$) δ 7.36−7.20 (m, 10H), 4.59 (s, 2H), 3.87−3.78 (m, 4H), 3.69 (s, 2H), 3.67−3.49 (m, 5H), 2.91−2.72 (m, 4H). MS (ESI) *m/z* 342 $[M + 1]^+$.

***N*-(*tert*-Butoxycarbonyl)-3,9-dioxa-6-azocyclodecan-1-ol (24).** A mixture of **23** (40 mg, 0.12 mmol), Boc_2O (26 mg, 0.12 mmol), and a catalytic amount of 10% Pd/C in EtOAc (3 mL) was stirred at 23 °C under a hydrogen atmosphere. After 18 h, the catalyst was filtered off and the filtrate was evaporated to afford 26 mg (95%) of **24** as a colorless oil. ^{1}H NMR ($CDCl_3$) δ 3.83−3.70 (m, 7H), 3.65−3.59 (m, 2H), 3.49−3.29 (m, 4H), 1.75 (bs, 1H), 1.46 (s, 9H). ^{13}C NMR ($CDCl_3$) δ 155.7, 79.8, 71.4, 71.0, 70.3, 69.9, 50.5, 50.2, 28.5.

(*S*)-1-(4-Nitrophenoxycarbonyloxy)-3,5-dioxacyclooctane (25a). To a solution of **8a** (15 mg, 0.11 mmol) and *N*-methylmorpholine (38 μL, 0.34 mmol) in dry THF (3 mL), *p*-nitrophenylchloroformate (70 mg, 0.28 mmol) was added and the resulting mixture was stirred at 23 °C for 1 h. To the reaction mixture was added water, the solvent was removed under reduced pressure, and the aqueous phase was extracted with $CHCl_3$. The organic extracts were dried (Na_2SO_4), and the solvent was removed. The residue was purified by flash-chromatography (1:4 EtOAc $CHCl_3$) to afford 28 mg (81%) of **25a** as a pale-yellow solid. ^{1}H NMR ($CDCl_3$) δ 8.27 (d, J = 9.3 Hz, 2H), 7.38 (d, J = 9.3 Hz, 2H), 5.09−5.01 (m, 1H), 4.72−4.66 (m, 2H), 3.94−3.82 (m, 3H), 3.64−3.56 (m, 1H), 2.18−2.04 (m, 1H), 2.03−1.93 (m, 2H), 1.90−1.71 (m, 1H).

(*S*)-1-(4-Nitrophenoxycarbonyloxy)-3,5-dioxacycloheptane (25b). The title compound was obtained from (*S*)-**8b** as described for **25a** in 72% yield. Flash-chromatography was performed using a 1:5 mixture of EtOAc and $CHCl_3$ as the eluant. ^{1}H NMR ($CDCl_3$) δ 8.28 (d, J = 9.3 Hz, 2H), 7.40 (d, J = 9.3 Hz, 2H), 5.00−4.98 (m, 1H), 4.84 (d, J = 4.5 Hz, 1H), 4.79 (d, J = 4.5 Hz, 1H), 4.11 (dd, J = 4.7, 13.1 Hz, 1H), 3.99−3.90 (m, 2H), 3.85−3.78 (m, 1H), 2.19−2.04 (m, 2H).

(*R*)-1-(4-Nitrophenoxycarbonyloxy)-3,5-dioxacyclooctane (25c). The title compound was obtained from (*R*)-**8c** as described for **25a** in 87% yield after flash-chromatography (1:4 EtOAc/$CHCl_3$). ^{1}H NMR data are consistent with those reported for the (*S*)-enantiomer **25a**.

(*R*)-1-(4-Nitrophenoxycarbonyloxy)-3,5-dioxacycloheptane (25d). The title compound was obtained from (*R*)-**8d** as described for **25a** in 70% yield after flash-chromatography (1:5 EtOAc/$CHCl_3$). ^{1}H data are consistent with those reported for the (*S*)-enantiomer **25b**.

(*R*)-3-(4-Nitrophenoxycarbonyloxy)oxepane (25e). The title compound was obtained from **8e** as described for **25a** in 86% yield. Flash-chromatography was performed using a 1:20 mixture of EtOAc and $CHCl_3$ as the eluant. ^{1}H NMR ($CDCl_3$) δ 8.26 (d, J = 9.3 Hz, 2H), 7.38 (d, J = 9.3 Hz, 2H), 5.02−4.95 (m, 1H), 3.98−3.83 (m, 3H), 3.71−3.63 (m, 1H), 2.15−1.74 (m, 5H), 1.65−1.53 (m, 1H).

(*S*)-4-(4-Nitrophenoxycarbonyloxy)oxepane (25f). The title compound was obtained from **8f** as described for **25a** in 77% yield. Flash-chromatography was performed using a 1:20 mixture of EtOAc and $CHCl_3$ as the eluant. ^{1}H NMR ($CDCl_3$) δ 8.27 (d, J = 8.8 Hz, 2H), 7.36 (d, J = 8.8 Hz, 2H), 5.05−5.01 (m, 1H), 3.84−3.62 (m, 4H), 2.18−1.86 (m, 5H), 1.78−1.63 (m, 1H).

1-(4-Nitrophenoxycarbonyloxy)cycloheptane (25g). The title compound was obtained from commercially available cycloheptanol as described for **25a** in 89% yield. Flash-chromatography was performed using a 1:10 mixture of EtOAc and $CHCl_3$ as the eluant. ^{1}H NMR ($CDCl_3$) δ 8.26 (d, J = 8.7 Hz, 2H), 7.37 (d, J = 8.7 Hz, 2H), 4.96−4.89 (m, 1H), 2.08−2.02 (m, 2H), 1.86−1.78 (m, 2H), 1.71 (m, 2H), 1.59 (m, 4H), 1.40−1.36 (m, 2H).

5-(4-Nitrophenoxycarbonyloxy)-1,3-dioxane (25h). The title compound was obtained from **8h** as described for **25a** in 72% yield. Flash-chromatography was performed using a 1:4 mixture of EtOAc and $CHCl_3$ as the eluant. ^{1}H NMR ($CDCl_3$) δ 8.30 (d, J = 8.7 Hz, 2H), 7.42 (d, J = 8.7 Hz, 2H), 5.03 (d, J = 6.3 Hz, 1H), 4.87 (d, J = 6.3 Hz, 1H), 4.71 (t, J = 2.8 Hz, 1H), 4.19−4.06 (m, 4H).

3,6,9-Trioxa-1-cyclodecanol succinimidylcarbonate (25i). To a solution of **8i** (18 mg, 0.11 mmol) in dry acetonitrile (1 mL), *N*,*N*′-disuccimidyl carbonate (43 mg, 0.17 mmol) and triethylamine (32 μL, 0.23 mmol) were added and the resulting mixture was stirred at 23 °C. After 8 h, the solvent was removed, the residue was taken up in a saturated solution of $NaHCO_3$, and the aqueous phase was extracted with EtOAc. The organic extracts were dried (Na_2SO_4), and the solvent was removed in vacuo. Purification of the residue (10:1 EtOAc/MeOH) afforded **17b** (13 mg) in 37% yield. ^{1}H NMR ($CDCl_3$) δ 5.12−5.03 (m, 1H), 3.96−3.65 (m, 12H), 2.81 (s, 4H).

12-(4-Nitrophenoxycarbonyloxy)-1,4,7,10-tetraoxacyclotridecane (25j). The title compound was obtained from **8j** as described for **25a** in 70% yield after flash-chromatography (EtOAc). ^{1}H NMR ($CDCl_3$) δ 8.27 (d, J = 9.3 Hz, 2H), 7.39 (d, J = 9.3 Hz, 2H), 5.15−5.08 (m, 1H), 3.92 (dd, J = 6.3, 10.2 Hz, 2H), 3.82 (dd, J = 4.5, 10.2 Hz, 2H), 3.74−3.60 (m, 12H).

9-(4-Nitrophenoxycarbonyloxy)-1,7-dioxa-4-thiacyclodecane 4,4-dioxide (25k). The title compound was obtained from **8k** as described for **25a** in 73% yield after flash-chromatography (1:4 EtOAc/$CHCl_3$). ^{1}H NMR ($CDCl_3$) δ 8.28 (d, J = 9.0 Hz, 2H), 7.37 (d, J = 9.0 Hz, 2H), 5.10−5.03 (m, 1H), 4.13−4.06 (m, 4H), 3.83−3.73 (m, 4H), 3.43−3.22 (m, 4H).

11-(4-Nitrophenoxycarbonyloxy)-1,4,6,9-tetraoxacyclododecane (25l). The title compound was obtained from **8l** as described for **25a** in 67% yield after flash-chromatography (EtOAc). ^{1}H NMR ($CDCl_3$) δ 8.27 (d, J = 8.7 Hz, 2H), 7.38 (d, J = 8.7 Hz, 2H), 5.01−4.95 (m, 1H), 4.70 (s, 2H), 3.91−3.76 (m, 12H).

(1*S*,2*R*)-{1-Benzyl-2-hydroxy-3-[isobutyl(4-methoxybenzenesulfonyl)amino]propyl}carbamic Acid (1*S*)-3,5-Dioxacyclooctan-1-yl ester (3a). A solution of **27** (25 mg, 0.05 mmol) in a mixture of 30% trifluoracetic acid in CH_2Cl_2 (5 mL) was stirred at 23 °C for 40 min and then the solvent was removed under reduced pressure. Compound **28** thus obtained was dissolved in CH_2Cl_2 (4 mL) and a solution of **25a** (16 mg, 0.05 mmol) in THF (2 mL) were added followed by diisopropylethylamine. After 48 h, the organic phase was washed with water, dried (Na_2SO_4), and

evaporated. The residue was purified by flash-chromatography eluting with a 1:4 mixture of EtOAc and hexane to afford **3a** in 63% yield after flash-chromatography (1:4 EtOAc/$CHCl_3$) as a foam: $[\alpha]_D^{20}$ +8.6 (*c* 1.1, $CHCl_3$). ^1H NMR ($CDCl_3$) δ 7.70 (d, J = 9.0 Hz, 2H), 7.31−7.21 (m, 5H), 6.97 (d, J = 9.0 Hz, 2H), 4.83−4.78 (m, 2H), 4.65−4.59 (m, 2H), 3.87 (s, 3H), 3.83−3.81 (m, 3H), 3.68 (dd, J = 4.9, 12.1 Hz, 1H), 3.55−3.48 (m, 2H), 3.14−2.90 (m, 5H), 2.78 (dd, J = 6.8, 12.6 Hz, 1H), 1.85−1.80 (m, 5H), 0.90 (d, J = 6.3 Hz, 3H), 0.85 (d, J = 6.3 Hz, 3H). ^{13}C NMR ($CDCl_3$) δ 163.0, 153.4, 137.6, 129.8, 129.6, 129.5, 128.4, 126.5, 114.3, 95.7, 73.9, 72.6, 69.2, 68.6, 58.7, 55.6, 55.0, 53.7, 35.4, 29.2, 27.2, 26.1, 20.1, 29.8. HRMS-ESI (*m/z*): $(M + Na)^+$ calcd for $C_{28}H_{40}N_2NaO_8S$, 587.2403; found, 587.2380.

(1*S*,2*R*)-{1-Benzyl-2-hydroxy-3-[isobutyl(4-methoxybenzenesulfonyl)amino]propyl}carbamic Acid (1*S*)-3,5-Dioxacycloheptan-1-yl Ester (3b). The title compound was obtained from **27** and **25b** as described for **3a** in 69% yield after flash-chromatography (1:4 EtOAc/$CHCl_3$) as an amorphous solid: $[\alpha]_D^{20}$ +10.5 (*c* 1.2, $CHCl_3$). ^1H NMR ($CDCl_3$) δ 7.70 (d, J = 8.7 Hz, 2H), 7.31−7.19 (m, 5H), 6.97 (d, J = 8.7 Hz, 2H), 4.93 (d, J = 8.4 Hz, 1H), 4.77−4.71 (m, 3H), 3.87 (s, 3H), 3.81−3.69 (m, 6H), 3.09−2.90 (m, 5H), 2.77 (dd, J = 6.9, 13.2 Hz, 1H), 1.98−1.95 (m, 1H), 1.85−1.76 (m, 2H), 0.90 (d, J = 6.9 Hz, 3H), 0.85 (d, J = 6.3 Hz, 3H). ^{13}C NMR ($CDCl_3$) δ 162.9, 155.5, 137.5, 129.7, 129.5, 129.4, 128.4, 126.5, 114.3, 94.9, 72.5, 71.9, 68.8, 62.3, 58.9, 55.6, 55.2, 53.7, 35.3, 27.3, 20.2, 19.9. HRMS-ESI (*m/z*): $(M + Na)^+$ calcd for $C_{27}H_{38}N_2NaO_8S$, 573.2247; found, 573.2260.

(1*S*,2*R*)-{1-Benzyl-2-hydroxy-3-[isobutyl(4-methoxybenzenesulfonyl)amino]propyl}carbamic Acid (1*R*)-3,5-Dioxacyclooctan-1-yl Ester (3c). The title compound was obtained from **27** and **25c** as described for **3a** in 50% yield after flash-chromatography (1:4 EtOAc/$CHCl_3$) as an amorphous solid $[\alpha]_D^{20}$ +9.8 (*c* 1.1, $CHCl_3$). ^1H NMR ($CDCl_3$) δ 7.70 (d, J = 8.7 Hz, 2H), 7.31−7.21 (m, 5H), 6.97 (d, J = 8.7 Hz, 2H), 4.80−4.79 (m, 2H), 4.65−4.61 (m, 2H), 3.87 (s, 3H), 3.82−3.80 (m, 2H), 3.71−3.62 (m, 2H), 3.56−3.48 (m, 2H), 3.12−2.85 (m, 5H), 2.77 (dd, J = 6.3, 13.2 Hz, 1H), 1.83−1.74 (m, 4H), 1.71−1.66 (m, 1H), 0.91 (d, J = 6.6 Hz, 3H), 0.86 (d, J = 6.6 Hz, 3H). HRMS-ESI (*m/z*): $(M + Na)^+$ calcd for $C_{28}H_{40}N_2NaO_8S$, 587.2403; found, 587.2405.

(1*S*,2*R*)-{1-Benzyl-2-hydroxy-3-[isobutyl(4-methoxybenzenesulfonyl)amino]propyl}carbamic Acid (1*R*)-3,5-Dioxacycloheptan-1-yl Ester (3d). The title compound was obtained from **27** and **25d** as described for **3a** in 59% yield after flash-chromatography (1:4 EtOAc/$CHCl_3$) as a foam: $[\alpha]_D^{20}$ +15.9 (*c* 0.6, $CHCl_3$). ^1H NMR ($CDCl_3$) δ 7.71 (d, J = 9.0 Hz, 2H), 7.30−7.18 (m, 5H), 6.98 (d, J = 9.0 Hz, 2H), 4.88 (d, J = 8.7 Hz, 1H), 4.77−4.71 (m, 3H), 3.87 (s, 3H), 3.81−3.61 (m, 6H), 3.18−3.07 (m, 2H), 3.04−2.92 (m, 2H), 2.86−2.74 (m, 2H), 1.90−1.77 (m, 3H), 0.92 (d, J = 6.3 Hz, 3H), 0.86 (d, J = 6.3 Hz, 3H). ^{13}C NMR ($CDCl_3$) δ 162.8, 155.5, 137.6, 129.7, 129.5, 129.4, 128.4, 126.4, 114.3, 94.8, 72.6, 71.9, 68.6, 62.3, 58.8, 55.6, 55.1, 53.8, 35.8, 35.2, 27.3, 20.2, 19.9. HRMS-ESI (*m/z*): $(M + Na)^+$ calcd for $C_{27}H_{38}N_2NaO_8S$, 573.2247; found, 573.2254.

(1*S*,2*R*)-{1-Benzyl-2-hydroxy-3-[isobutyl(4-methoxybenzenesulfonyl)amino]propyl}carbamic Acid (*R*)-Oxepan-3-yl Ester (3e). The title compound was obtained from **27** and **25e** as described for **3a** in 72% yield after flash-chromatography (1:2 EtOAc/hex) as an amorphous solid. ^1H NMR ($CDCl_3$) δ 7.70 (d, 8.8 Hz, 2H), 7.30−7.19 (m, 5H), 6.97 (d, J = 8.8 Hz, 2H), 4.81 (d, J = 8.2 Hz, 1H), 4.77−4.74 (m, 1H), 3.87 (s, 3H), 3.81 (m, 3H), 3.70−3.69 (m, 2H), 3.61−3.57 (m, 1H), 3.12 (dd, J = 8.2, 14.7 Hz, 1H), 3.05−3.84 (m, 4H), 2.77 (dd, J = 6.6, 13.2 Hz, 1H), 1.86−1.60 (m, 6H), 1.49−1.41 (m, 1H), 0.91 (d, J = 6.7 Hz, 3H), 0.86 (d, J = 6.7 Hz, 3H). ^{13}C NMR ($CDCl_3$) δ 162.9, 155.8, 137.5, 129.6, 129.5, 129.4, 128.4, 126.4, 114.2, 74.5, 73.6, 72.5, 72.4, 58.7, 55.5, 54.8, 53.7, 35.6, 31.9, 30.9, 27.1, 21.0, 20.0, 19.8. HRMS-ESI (*m/z*): $(M + Na)^+$ calcd for $C_{28}H_{40}N_2NaO_7S$, 571.2454; found, 571.2458.

(1*S*,2*R*)-{1-Benzyl-2-hydroxy-3-[isobutyl(4-methoxybenzenesulfonyl)amino]propyl}carbamic acid (*S*)-oxepan-4-yl ester (3f). The title compound was obtained from **27** and **25f** as described for **3a** in 68% yield after flash-chromatography (1:2 EtOAc/hex) as an amorphous solid. ^1H NMR ($CDCl_3$) δ 7.71 (d, J = 8.8 Hz, 2H), 7.29−7.21 (m, 5H), 6.98 (d, J = 8.8 Hz, 2H), 4.78−4.76 (m, 2H), 3.94−3.81 (m, 5H), 3.71−3.60 (m, 3H), 3.56−3.50 (m, 1H), 3.12 (dd, J = 8.0, 15.2 Hz, 1H), 3.04−2.86 (m, 4H), 2.79 (dd, J = 6.4, 13.1 Hz, 1H), 1.94−1.64 (m, 7H), 0.91 (d, J = 6.5 Hz, 3H), 0.86 (d, J = 6.5 Hz, 3H). HRMS-ESI (*m/z*): $(M + Na)^+$ calcd for $C_{28}H_{40}N_2NaO_7S$, 571.2454; found, 571.2452.

(1*S*,2*R*)-{1-Benzyl-2-hydroxy-3-[isobutyl(4-methoxybenzenesulfonyl)amino]propyl}carbamic Acid Cycloheptanyl Ester (3g). The title compound was obtained from **27** and **25g** as described for **3a** in 84% yield after flash-chromatography (1:6 EtOAc/$CHCl_3$) as an amorphous solid: $[\alpha]_D^{20}$ +16.0 (*c* 0.9, $CHCl_3$). ^1H NMR ($CDCl_3$) δ 7.70 (d, J = 8.7 Hz, 2H), 7.31−7.22 (m, 5H), 6.97 (d, J = 8.7 Hz, 2H), 4.69−4.68 (m, 2H), 3.87 (s, 3H), 3.82−3.78 (m, 2H), 3.05−2.77 (m, 6H), 1.83−1.73 (m, 4H), 1.60−1.45 (m, 8H), 1.22−1.20 (m, 1H), 0.90 (d, J = 6.3 Hz, 3H), 0.86 (d, J = 6.3 Hz, 3H). HRMS-ESI (*m/z*): $(M + Na)^+$ calcd for $C_{29}H_{42}N_2NaO_6S$, 569.2661; found, 569.2663.

(1*S*,2*R*)-{1-Benzyl-2-hydroxy-3-[isobutyl(4-methoxybenzenesulfonyl)amino]propyl}carbamic Acid 1,3-Dioxan-5-yl Ester (3h). The title compound was obtained from **25h** and **27** as described for **3a** in 67% yield after flash-chromatography (1:6 EtOAc/$CHCl_3$): $[\alpha]_D^{20}$ +7.9 (12.3 mg/mL CH_2Cl_2). ^1H NMR ($CDCl_3$) δ 7.71 (d, J = 9.3 Hz, 2H), 7.32−7.22 (m, 5H), 6.98 (d, J = 9.3 Hz, 2H), 5.06 (d, J = 8.4 Hz, 1H), 4.92 (d, J = 6.2 Hz, 1H), 4.75 (d, J = 6.2 Hz, 1H), 4.51−4.49 (m, 1H), 3.95−3.74 (m, 9H), 3.14 (dd, J = 8.1, 15.0 Hz, 1H), 3.06−2.84 (m, 4H), 2.77 (dd, J = 6.7, 13.3 Hz, 1H), 1.86−1.77 (m, 1H), 0.92 (d, J = 6.6 Hz, 3H), 0.87 (d, J = 6.6 Hz, 3H). ^{13}C NMR ($CDCl_3$) δ 162.9, 155.4, 137.3, 129.7, 129.6, 129.5, 128.5, 126.5, 114.3, 93.6, 72.3, 68.7, 66.3, 58.8, 55.6, 55.2, 53.8, 35.7, 27.3, 20.2, 19.9. HRMS-ESI (*m/z*): $(M + Na)^+$ calcd for $C_{26}H_{36}N_2NaO_8S$, 559.2090; found, 559.2094.

(1*S*,2*R*)-(1-Benzyl-2-hydroxy-3-[isobutyl(4-methoxybenzenesulfonyl)amino]propyl)carbamic Acid 3,6,9-Trioxacyclodecan-1-yl Ester (3i). The title compound was obtained from **25i** and **27** as described for **3a** in 37% yield after flash-chromatography (1:1 EtOAc/$CHCl_3$) as a white solid: mp 60−62 °C; $[\alpha]_D^{20}$ + 6.2 (*c* 0.3, $CHCl_3$). ^1H NMR ($CDCl_3$) δ 7.69 (d, J = 8.7 Hz, 2H), 7.33−7.18 (m, 5H), 6.96 (d, J = 8.7 Hz, 2H), 5.33 (d, J = 8.1 Hz, 1H), 4.84−4.82 (m, 1H), 3.86 (s, 3H), 3.79−3.75 (m, 2H), 3.68−3.55 (m, 12H), 3.07−2.78 (m, 6H), 1.84−1.81 (m, 1H), 0.89 (d, J = 7.2 Hz, 3H), 0.85 (d, J = 7.2 Hz, 3H). HRMS-ESI (*m/z*): $(M + Na)^+$ calcd for $C_{29}H_{42}N_2NaO_9S$, 617.2509; found, 617.2501.

(1*S*,2*R*)-{1-Benzyl-2-hydroxy-3-[isobutyl(4-methoxybenzenesulfonyl)amino]propyl}carbamic Acid 3,6,9,12-Tetraoxacyclotridecan-1-yl Ester (3j). The title compound was obtained from **27** and **25j** as described for **3a** in 30% yield after flash-chromatography (EtOAc) as a foam: $[\alpha]_D^{20}$ +17.0 (*c* 0.9, $CHCl_3$). ^1H NMR ($CDCl_3$) δ 7.70 (d, J = 9.0 Hz, 2H), 7.29−7.19 (m, 5H), 6.97 (d, J = 9.0 Hz, 2H), 4.96 (d, J = 8.0 Hz, 1H), 4.85−4.83 (m, 1H), 3.87 (s, 3H), 3.83−3.81 (m, 2H), 3.80−3.60 (m, 15H), 3.52 (dd, J = 3.5, 9.5 Hz, 1H), 3.13 (dd, J = 9.0, 15.5 Hz, 1H), 3.02−2.86 (m, 4H), 2.77 (dd, J = 6.5, 13.5 Hz, 1H), 1.83−1.76 (m, 1H), 0.90 (d, J = 6.5 Hz, 3H), 0.85 (d, J = 6.5 Hz, 3H). ^{13}C NMR ($CDCl_3$) (500 MHz) δ 163.0, 155.4, 137.6, 129.7, 129.6, 129.5, 128.5, 126.5, 114.4, 72.4, 71.7, 70.2, 70.1, 69.9, 67.8, 58.7, 55.6, 55.1, 53.7, 35.5, 27.3, 20.2, 19.9. HRMS-ESI (*m/z*): $(M + Na)^+$ calcd for $C_{31}H_{46}N_2NaO_{10}S$, 661.2771; found, 661.2788.

(1*S*,2*R*)-{1-Benzyl-2-hydroxy-3-[isobutyl(4-methoxybenzenesulfonyl)amino]propyl}carbamic Acid 3,6,8,11-Tetraoxacyclododecan-1-yl Ester (3k). The title compound was obtained from **27** and **25k** as described for **3a** in 47% yield after flash-chromatography (EtOAc) as a foam: $[\alpha]_D^{20}$ +6.5 (*c* 0.5, $CHCl_3$). ^1H NMR ($CDCl_3$) 7.70 (d, J = 8.7 Hz, 2H), 7.30−7.18 (m, 5H), 6.97 (d, J = 8.7 Hz, 2H), 4.92 (d, J = 8.1 Hz, 1H), 4.81−4.76 (m, 1H), 4.66 (s, 2H), 3.87 (s, 3H), 3.78−344 (m, 14H), 3.13 (dd, J =

8.4, 15.3 Hz, 1H), 3.06−2.82 (m, 4H), 2.75 (dd, J = 6.9, 13.5 Hz, 1H), 1.83−1.74 (m, 1H), 0.90 (d, J = 6.6 Hz, 3H), 0.85 (d, J = 6.3 Hz, 3H). ^{13}C NMR ($CDCl_3$) δ 163.0, 155.6, 137.5, 129.8, 129.6, 129.5, 128.5, 126.5, 114.4, 94.7, 72.4, 71.5, 69.7, 64.9, 64.5, 58.8, 55.7, 55.1, 53.8, 35.6, 27.3, 20.2, 19.9. HRMS-ESI (m/z): (M + Na)$^+$ calcd for $C_{30}H_{44}N_2NaO_{10}S$, 647.2615; found, 647.2590.

(1*S*,2*R*)-{1-Benzyl-2-hydroxy-3-[isobutyl(4-methoxybenzenesulfonyl)amino]propyl}carbamic Acid 3,9-Dioxa-6-thiacyclodecan-1-yl 6,6-Dioxide Ester (3l). The title compound was obtained from **27** and **25l** as described for **3a** in 36% yield after flash-chromatography (1:1 EtOAc/$CHCl_3$) as an amorphous solid: $[\alpha]_D^{20}$ +5.5 (c 0.7, $CHCl_3$). ^{1}H NMR ($CDCl_3$) δ 7.70 (d, J = 9.0 Hz, 2H), 7.31−7.20 (m, 5H), 6.98 (d, J = 9.0 Hz, 2H), 4.97 (d, J = 8.4 Hz, 1H), 4.85 (t, J = 4.5 Hz, 1H), 4.01−3.96 (m, 4H), 3.88 (s, 3H), 3.85−3.83 (m, 2H), 3.71−3.69 (m, 1H), 3.61 (dd, J = 3.9, 9.3 Hz, 1H), 3.54−3.47 (m, 2H), 3.61−3.27 (m, 4H), 3.13 (dd, J = 8.4, 15.0 Hz, 1H), 3.00−2.82 (m, 4H), 2.75 (dd, J = 6.6, 13.5 Hz, 1H), 1.83−1.75 (m, 1H), 0.91 (d, J = 6.6 Hz, 3H), 0.86 (d, J = 6.3 Hz, 3H). ^{13}C NMR ($CDCl_3$) δ 163.0, 155.1, 137.4, 131.1, 129.6, 129.4, 128.4, 126.5, 114.3, 72.4, 70.2, 66.0, 64.6, 58.8, 55.7, 55.1, 53.7, 52.2, 35.4, 27.3, 20.2, 19.9. HRMS-ESI (m/z): (M + Na)$^+$ calcd for $C_{29}H_{42}N_2NaO_{10}S_2$, 665.2179; found, 665.2191.

***N*-(*tert*-Butoxycarbonyl)-9-(4-nitrophenoxycarbonyloxy)-1,7-dioxa-4-azocyclodecane (29).** The title compound was obtained from **24** as described for **25a** in 73% yield after flash-chromatography (1:4 EtOAc/$CHCl_3$). ^{1}H NMR ($CDCl_3$) δ 8.27 (d, J = 9.0 Hz, 2H), 7.37 (d, J = 9.0 Hz, 2H), 5.02−4.96 (m, 1H), 3.98−3.76 (m, 8H), 4.52−3.23 (m, 4H), 1.47 (s, 9H).

(1*S*,2*R*)-{1-Benzyl-2-hydroxy-3-[isobutyl(4-methoxybenzenesulfonyl)amino]propyl}carbamic Acid *N*-(*tert*-Butoxycarbonyl)-1,7-dioxa-4-azocyclodecan-9-yl Ester (30). The title compound was obtained from **27** and **29** as described for **3a** in 74% yield after flash-chromatography (1:1 EtOAc/$CHCl_3$) as a white solid: mp 71−73 °C; $[\alpha]_D^{20}$ +4.7 (c 1.7, $CHCl_3$). ^{1}H NMR ($CDCl_3$) 7.70 (d, J = 9.0 Hz, 2H), 7.30−7.20 (m, 5H), 7.0 (d, J = 9.0 Hz, 2H), 4.92−4.90 (m, 1H), 4.81 (t, J = 4.0 Hz, 1H), 3.86 (s, 3H), 3.79−3.66 (m, 6H), 3.62−3.57 (m, 2H), 3.49−3.42 (m, 2H), 3.40−3.28 (m, 4H), 3.12 (dd, J = 7.8, 15.3 Hz, 1H), 3.01−2.82 (m, 4H), 2.75 (dd, J = 6.3, 13.2 Hz, 1H), 1.83−1.74 (m, 1H), 1.44 (s, 9H), 0.90 (d, J = 6.6 Hz, 3H), 0.85 (d, J = 6.6 Hz, 3H). ^{13}C NMR ($CDCl_3$) 163.0, 155.6, 155.4, 137.4, 129.7, 129.5, 129.4, 128.4, 126.5, 114.3, 79.9, 72.4, 71.9, 71.0, 68.6, 68.1, 58.7, 55.6, 55.0, 53.7, 50.3, 35.6, 28.5, 27.3, 20.2, 19.9.

(1*S*,2*R*)-{1-Benzyl-2-hydroxy-3-[isobutyl(4-methoxybenzenesulfonyl)amino]propyl}carbamic Acid 1,7-Dioxa-4-azocyclodecan-9-yl Ester (31). A solution of **30** (13 mg, 0.02 mmol) in a mixture of 30% trifluoracetic acid in CH_2Cl_2 (1 mL) was stirred at 23 °C for 30 min and then the solvent was removed under reduced pressure. The residue was dissolved in CH_2Cl_2, and the organic phase was washed with a saturated solution of $NaHCO_3$, dried (Na_2SO_4), and evaporated to afford 11 mg (100%) of **31** as a white solid: mp 65−66 °C; $[\alpha]_D^{20}$ +13.8 (c 0.7, $CHCl_3$). ^{1}H NMR ($CDCl_3$) δ 7.70 (d, J = 8.7 Hz, 2H), 7.30−7.18 (m, 5H), 6.97 (d, J = 8.7 Hz, 2H), 5.20 (d, J = 8.4 Hz, 1H), 4.82−4.79 (m, 1H), 3.87 (s, 3H), 3.84−3.80 (m, 2H), 3.75−3.64 (m, 7H), 3.54 (dd, J = 5.4, 10.2 Hz, 1H), 3.13 (dd, J = 8.4, 15.3 Hz, 1H), 3.04−2.84 (m, 8H), 2.77 (dd, J = 6.9, 13.5 Hz, 1H), 2.38 (bs, 1H), 1.85−1.76 (m, 1H), 0.90 (d, J = 6.3 Hz, 3H), 0.85 (d, J = 6.6 Hz, 3H). ^{13}C NMR ($CDCl_3$) δ 162.9, 155.3, 137.5, 129.8, 129.5, 129.4, 128.4, 126.4, 114.3, 72.4, 71.8, 68.6, 58.7, 55.6, 55.1, 53.6, 53.4, 48.2, 35.6, 27.2, 20.2, 19.9.

(1*S*,2*R*)-{1-Benzyl-2-hydroxy-3-[isobutyl(4-methoxybenzenesulfonyl)amino]propyl}carbamic Acid *N*-Methyl-1,7-dioxa-4-azocyclodecan-9-yl Ester (3m). To a solution of **31** (9.0 mg, 0.015 mmol) in a mixture of 1% acetic acid in methanol (0.5 mL), formaldehyde (37% solution in H_2O, 12 μL, 0.15 mmol), and sodium cyanoborohydride (2.0 mg, 0.03 mmol) were added. After 18 h, a saturated solution of $NaHCO_3$ was added, the solvent was removed and the aqueous phase was extracted with CH_2Cl_2. The organic extracts were dried (Na_2SO_4), evaporated, and the residue was purified by flash-chromatography eluting with a 10:1 mixture of $CHCl_3$ and MeOH to afford 8.0 mg (87%) of **3m** as an amorphous solid: $[\alpha]_D^{20}$ +8.1 (c 0.6, $CHCl_3$). ^{1}H NMR ($CDCl_3$) δ 7.70 (d, J = 8.7 Hz, 2H), 7.3−7.18 (m, 5H), 6.98 (d, J = 8.7 Hz, 2H), 4.99 (d, J = 8.1 Hz, 1H), 4.80−4.77 (m, 1H), 3.87 (s, 3H), 3.83−3.74 (m, 4H), 3.70−3.56 (m, 6H) 3.14 (dd, J = 8.1, 14.7 Hz, 1H), 3.02−2.69 (m, 9H), 2.40 (s, 3H), 1.83−1.74 (m, 1H), 0.90 (d, J = 6.3 Hz, 3H), 0.85 (d, J = 6.6 Hz, 3H). ^{13}C NMR ($CDCl_3$) δ 162.9, 155.5, 137.4, 129.9, 129.4 (×2C), 128.4, 126.4, 114.3, 77.2, 72.3, 69.6, 67.6, 59.0, 55.6, 55.1, 53.6, 44.0, 35.6, 29.7, 27.2, 20.2, 19.9. HRMS-ESI (m/z): (M + Na)$^+$ calcd for $C_{30}H_{46}N_3O_8S$, 608.3006; found, 608.3009.

Determination of X-ray Structure of 3d-Bound HIV Protease. The HIV-1 protease construct with the substitutions Q7K, L33I, L63I, C67A, and C95A to optimize protein stability[33] was expressed and purified as described.[34] Crystals were grown by the hanging drop vapor diffusion method using a 1:15 molar ratio of protease at 2.0 mg/mL and inhibitor dissolved in dimethylsulfoxide. The reservoir contained 0.1 M sodium acetate buffer (pH = 4.2) and 1.2 M NaCl, 10% DMSO. Crystals were transferred into a cryoprotectant solution containing the reservoir solution and 20−30% (v/v) glycerol, mounted on a nylon loop and flash-frozen in liquid nitrogen. X-ray diffraction data were collected on the SER-CAT beamline of the Advanced Photon Source, Argonne National Laboratory. Diffraction data were processed using HKL2000,[35] resulting in an R_{merge} value of 8.0% (41.1%) for 110362 unique reflections between 50 and 1.00 Å resolution with a completeness of 88.4% (52.6%), where the values in parentheses are for the final highest resolution shell. Data were reduced in space group $P2_12_12$ with unit cell dimensions of a = 57.96 Å, b = 86.41 Å, c = 46.03 Å with one dimer in the asymmetric unit. The structure was solved by molecular replacement using the CPP4i suite of programs,[36,37] with the structure of the D30N mutant of HIV protease in complex with GRL-98065 (2QCI)[34] as the starting model. The structure was refined using SHELX97[38] and refitted manually using the molecular graphics programs O[39] and COOT.[40] Alternate conformations were modeled for the protease residues when obvious in the electron density maps. Anisotropic atomic displacement parameters (B-factors) were refined for all atoms including solvent molecules. Hydrogen atoms were added at the final stages of the refinement. The identity of ions and other solvent molecules from the crystallization conditions was deduced from the shape and peak height of the $2F_o - F_c$ and $F_o - F_c$ electron density, the hydrogen bond interactions, and interatomic distances. The solvent structure was refined with two sodium ions, three chloride ions, and 219 water molecules including partial occupancy sites. The final R_{work} was 14.7% and R_{free} was 17.5% for all data between 10 and 1.00 Å resolution. The rmsd values from ideal bonds and angle distances were 0.017 Å and 0.034 Å, respectively. The average B-factor was 11.4 and 16.5 Å^2 for protease main chain and side chain atoms, respectively, 12.9 Å^2 for inhibitor atoms, and 22.6 Å^2 for solvent atoms. The X-ray crystal structure of the **3d**-bound HIV-1 protease has been deposited in the Protein Data Bank (PDB)[41] with accession code 3DJK.

Acknowledgment. This research was supported by grants from the National Institutes of Health (GM53386, A.K.G., and GM62920, I.W.). This work was also supported by the Intramural Research Program of the Center for Cancer Research, National Cancer Institute, National Institutes of Health and in part by a Grant-in-aid for Scientific Research (Priority Areas) from the Ministry of Education, Culture, Sports, Science, and Technology of Japan (Monbu Kagakusho), a Grant for Promotion of AIDS Research from the Ministry of Health, Welfare, and Labor of Japan (Kosei Rohdosho: H15-AIDS-001), and the Grant to the Cooperative Research Project on Clinical and Epidemiological Studies of Emerging and Re emerging Infectious Diseases (Renkei Jigyo: no. 78, Kumamoto University) of Monbu-Kagakusho. The work was also supported in part by the Georgia State University Molecular Basis of Disease

Program, the Georgia Research Alliance, the Georgia Cancer Coalition. We thank the staff at the SER-CAT beamline at the Advanced Photon Source, Argonne National Laboratory, for assistance during X-ray data collection. Use of the Advanced Photon Source was supported by the U.S. Department of Energy, Office of Science, Office of Basic Energy Sciences, under contract no. DE-AC02-06CH11357. We also thank Sofiya Leshchenko-Yashchuk for her assistance in HIV-1 protease inhibitory assay.

Supporting Information Available: HPLC and HRMS data of inhibitors **3a**−**m**; crystallographic data collection and refinement statistics. This material is available free of charge via the Internet at http://pubs.acs.org.

References

(1) Sepkowitz, K. A. AIDS—The first 20 years. *Engl. J. Med.* **2001**, *344*, 1764–1772.

(2) Waters, L.; Nelson, M. Why do patients fail HIV therapy? *Int. J. Clin. Pract.* **2007**, *61*, 983–990.

(3) Pillay, D.; Bhaskaran, K.; Jurriaans, S.; Prins, M.; Masquelier, B.; Dabis, F.; Gifford, R.; Nielsen, C.; Pedersen, C.; Balotta, C.; Rezza, G.; Ortiz, M.; de Mendoza, C.; Kücherer, C.; Poggensee, G.; Gill, J.; Porter, K. The impact of transmitted drug resistance on the natural history of HIV infection and response to first-line therapy. *AIDS* **2006**, *20*, 21–28.

(4) Grabar, S.; Pradier, C.; Le Corfec, E.; Lancar, R.; Allavena, C.; Bentata, M.; Berlureau, P.; Dupont, C.; Fabbro-Peray, P.; Poizot-Martin, I.; Costagliola, D. Factors associated with clinical and virological failure in patients receiving a triple therapy including a protease inhibitor. *AIDS* **2000**, *14*, 141–149.

(5) Wainberg, M. A.; Friedland, G. Public health implications of antiretroviral therapy and HIV drug resistance. *J. Am. Med. Assoc.* **1998**, *279*, 1977–1983.

(6) Harrigan, P. R.; Hogg, R. S.; Dong, W. W.; Yip, B.; Wynhoven, B.; Woodward, J.; Brumme, C. J.; Brumme, Z. L.; Mo, T.; Alexander, C. S.; Montaner, J. S. Predictors of HIV drug-resistance mutations in a large antiretroviral naive cohort initiating triple antiretroviral therapy. *J. Infect. Dis.* **2005**, *191*, 339–347.

(7) Hertogs, K.; Bloor, S.; Kemp, S. D.; Van den Eynde, C.; Alcorn, T. M.; Pauwels, R.; Van Houtte, M.; Staszewski, S.; Miller, V.; Larder, B. A Phenotypic and genotypic analysis of clinical HIV-1 isolates reveals extensive protease inhibitor cross-resistance: a survey of over 6000 samples. *AIDS* **2000**, *14*, 1203–1210.

(8) Yerly, S.; Kaiser, L.; Race, E.; Bru, J. P.; Clavel, F.; Perrin, L. Transmission of antiretroviral drug resistant HIV-1 variants. *Lancet* **1999**, *354*, 729–733.

(9) On June 23, 2006, FDA approved new HIV treatment for patients who do not respond to existing drugs. Please see: http://www.fda.gov/bbs/topics/NEWS/2006/NEW01395.html.

(10) Ghosh, A. K.; Kincaid, J. F.; Cho, W.; Walters, D. E.; Krishnan, K.; Hussain, K. A.; Koo, Y.; Cho, H.; Rudall, C.; Holland, L.; Buthod, J. Potent HIV protease inhibitors incorporating high-affinity P2-ligands and (*R*)-(hydroxyethylamino)sulfonamide isostere. *Bioorg. Med. Chem. Lett.* **1998**, *8*, 687–690.

(11) Koh, Y.; Nakata, H.; Maeda, K.; Ogata, H.; Bilcer, G.; Devasamudram, T.; Kincaid, J. F.; Boross, P.; Wang, Y.-F.; Tie, Y.; Volarath, P.; Gaddis, L.; Harrison, R. W.; Weber, I. T.; Ghosh, A. K.; Mitsuya, H. A novel bis-tetrahydrofuranylurethane-containing non-peptide protease inhibitor (PI) UIC-94017 (TMC-114) potent against multi-PI-resistant HIV in vitro. *Antimicrob. Agents Chemother.* **2003**, *47*, 3123–3129.

(12) Surleraux, D. L. N. G.; Tahri, A.; Verschueren, W. G.; Pille, G. M. E.; de Kock, H. A.; Jonckers, T. H. M.; Peeters, A.; De Meyer, S.; Azijn, H.; Pauwels, R.; de Bethune, M.-P.; King, N. M.; Prabu-Jeyabalan, M.; Schiffer, C. A.; Wigerinck, P. B. T. P. Discovery and selection of TMC114, a next generation of HIV-1 protease inhibitor. *J. Med. Chem.* **2005**, *48*, 1813–1822.

(13) Yoshimura, K.; Kato, R.; Kavlick, M. F.; Nguyen, A.; Maroun, V.; Maeda, K.; Hussain, K. A.; Ghosh, A. K.; Gulnik, S. V.; Erickson, J. W.; Mitsuya, H. A potent human immunodeficiency virus type 1 protease inhibitor, UIC-94003 (TMC-126), and selection of a novel (A28S) mutation in the protease active Site. *J. Virol.* **2002**, *76*, 1349–1358.

(14) (a) Kohl, Y.; Maeda, K.; Ogata, H.; Bilcer, G.; Devasamudram, T.; Kincaid, J. F.; Boross, P.; Wang, Y.-F.; Tie, Y.; Volarath, P.; Gaddis, L.; Louis, J. M.; Harrison, R. W.; Weber, I. T.; Ghosh, A. K.; Mitsuya, H. Novel bis-tetrahydrofuranyl-urethane-containing nonpeptidic protease inhibitor (PI) UIC-94017 (TMC114) potent against multi-PI-resistant human immunodeficiency virus in vitro. *Antimicrob. Agents Chemother* **2003**, *47*, 3123–3129. (b) Ghosh, A. K.; Pretzer, E.; Cho, H.; Hussain, K. A.; Duzgunes, N. Antiviral activity of UIC-PI, a novel inhibitor of the human immunodeficiency virus type 1 protease. *Antiviral Res.* **2002**, *54*, 29–36.

(15) Tie, Y.; Boross, P. I.; Wang, Y.-F.; Gaddis, L.; Hussain, A. K.; Leshchenko, S.; Ghosh, A. K.; Louis, J. M.; Harrison, R. W.; Weber, I. T. High-resolution crystal structures of HIV-1 protease with a potent non-peptide inhibitor (UIC-94017) active against multidrug-resistant clinical strains. *J. Mol. Biol.* **2004**, *338*, 341–352.

(16) Hong, L.; Zhang, X. C.; Hartsuck, J. A.; Tang, J. Crystal structure of an in vivo HIV-1 protease mutant in complex with saquinavir: Insights into the mechanisms of drug resistance. *Protein Sci.* **2000**, *9*, 1989–1904.

(17) Laco, G. S.; Schalk-Hihi, C.; Lubkowski, J.; Morris, G.; Zdanov, A.; Olson, A.; Elder, J. H.; Wlodawer, A.; Gustchina, A. Crystal Structures of the Inactive D30N Mutant of Feline Immunodeficiency Virus Protease Complexed with a Substrate and an Inhibitor. *Biochemistry* **1997**, *36*, 10696–10708.

(18) Winitz, M.; Bloch-Frankenthal, L.; Izumiya, N.; Birnbaum, S. M.; Baker, C. G.; Greenstein, J. P. Studies on Diastereoisomeric α-Amino Acids and Corresponding α-Hydroxy Acids. VII. *J. Am. Chem. Soc.* **1956**, *78*, 2423–2430.

(19) Soai, K.; Ookawa, A. Mixed solvents containing methanol as useful reaction media for unique chemoselective reductions with lithium borohydride. *J. Org. Chem.* **1986**, *51*, 4000–4005.

(20) Gmeiner, P.; Junge, D. Regioselective transformation of malic acid: a practical method for the construction of enantiomerically pure indolizidines. *J. Org. Chem.* **1995**, *60*, 3910–3915.

(21) Le Merrer, Y.; Gauzy, L.; Gravier-Pelletier, C.; Depezay, J.-C. Synthesis of C_2-symmetric guanidino-sugars as potent inhibitors of glycosidases. *Bioorg. Med. Chem.* **2000**, *8*, 307–320.

(22) Pospíšil, J.; Markó, I. E. Total synthesis of (*R*)-(+)-goniothalamin and (*R*)-(+)-goniothalamin oxide: first application of the sulfoxide-modified Julia olefination in total synthesis. *Tetrahedron Lett.* **2007**, *47*, 5933–5937.

(23) Lu, C.-D.; Zakarian, A. Studies toward the synthesis of pinnatoxins: The B,C,D-dispiroketal fragment. *Org. Lett.* **2007**, *9*, 3161–3163.

(24) Kasireddy, K.; Ahmad, M. U.; Ali, S. M.; Ahmad, I. Synthesis of novel cationic cardiolipin analogues for the optimal delivery of therapeutic agents. *Tetrahedron Lett.* **2004**, *45*, 2743–2746.

(25) Calverley, M. J.; Dale, J. 1,4,7-Trioxa-10-azacyclododecane and some N-substituted derivatives; synthesis and cation complexing. *Acta Chem. Scand.* **1982**, *B36*, 241–247.

(26) Sakamoto, H.; Kimura, K.; Koseki, Y.; Matsuo, M.; Shono, T. Lipophilic bis(monoaza crown ether) derivatives: synthesis and cation-complexing properties. *J. Org. Chem.* **1986**, *51*, 4974–4979.

(27) Ghosh, A. K.; Fidanze, S. Transition-state mimetics for HIV protease inhibitors: stereocontrolled synthesis of hydroxyethylene and hydroxyethylamine isosteres by ester-derived titanium enolate *syn*- and *anti*-aldol reactions. *J. Org. Chem.* **1998**, *63*, 6146–6152.

(28) Toth, M. V.; Marshall, G. R. A simple, continuous fluorometric assay for HIV protease. *Int. J. Pep. Protein Res.* **1990**, *36*, 544–550.

(29) Gustchina, A.; Sansom, C.; Prevost, M.; Richelle, J.; Wodak, S.; Wlodawer, A.; Weber, I. Energy calculations and analysis of HIV-1 protease-inhibitor crystal structures. *Protein Eng.* **1994**, *7*, 309–317.

(30) Tie, Y.; Boross, P. I.; Wang, Y. F.; Gaddis, L.; Liu, F.; Chen, X.; Tozser, J.; Harrison, R. W.; Weber, I. T. Molecular basis for substrate recognition and drug resistance from 1.1 to 1.6 Angstroms resolution crystal structures of HIV-1 protease mutants with substrate analogs. *FEBS J.* **2005**, *272*, 5265–5277.

(31) Wang, Y. F.; Tie, Y.; Boross, P. I.; Tozser, J.; Ghosh, A. K.; Harrison, R. W.; Weber, I. T. Potent new antiviral compound shows similar inhibition and structural interactions with drug resistant mutants and wild type HIV-1 protease. *J. Med. Chem.* **2007**, *50*, 4509–4515.

(32) Hronowski, L. J. J.; Szarek, W. A.; Hay, G. W.; Krebs, A.; Depew, W. T. Synthesis and characterization of 1-*O*-β-lactosyl-(*R*,*S*)-glycerols and 1,3-di-*O*-β-lactosylglycerol. *Carbohydr. Res.* **1989**, *190*, 203–218.

(33) Louis, J. M.; Clore, G. M.; Gronenborn, A. M. Autoprocessing of HIV-1 protease is tightly coupled to protein folding. *Nat. Struct. Biol.* **1999**, *6*, 868–875.

(34) Mahalingam, B.; Louis, J. M.; Hung, J.; Harrison, R. W.; Weber, I. T. Structural implications of drug resistant mutants of HIV-1 protease: High resolution crystal structures of the mutant protease/substrate analog complexes. *Proteins* **2001**, *43*, 455–464.

(35) Otwinowski, Z.; Minor, W. Processing of X-ray diffraction data in oscillation mode. *Methods Enzymol.* **1997**, *276*, 307–326.

(36) Collaborative Computational Project, Number 4. The CCP4 Suite: Programs for Protein Crystallography. *Acta Crystallogr., Sect. D: Biol. Crystallogr.* **1994**, *50*, 760−763.

(37) Potterton, E.; Briggs, P.; Turkenburg, M.; Dodson, E. A graphical user interface to the CCP4 program suite. *Acta Crystallogr., Sect. D: Biol. Crystallogr.* **2003**, *59*, 1131–1137.
(38) Sheldrick, G. M.; Schneider, T. R. SHELXL: High resolution refinement. *Methods Enzymol.* **1997**, *277*, 319–343.
(39) Jones, T. A.; Zou, J. Y.; Cowan, S. W.; Kjeldgaard, M. Improved methods for building protein models in electron density maps and the location of errors in these models. *Acta Crystallogr., Sect A: Found. Crystallogr.* **1991**, *47*, 110–119.
(40) Emsley, P.; Cowtan, K. Coot: Model-Building Tools for Molecular Graphics. *Acta Crystallogr., Sect. D: Biol. Crystallogr.* **2004**, *60*, 2126–2132.
(41) Berman, H. M.; Westbrook, J.; Feng, Z.; Gilliland, G.; Bhat, T. N.; Weissig, H.; Shindyalov, I. N.; Bourne, P. E. The Protein Data Bank. *Nucleic Acids Res.* **2000**, *28*, 235–242.
(42) (a) Shirasaka, T.; Yarchoan, R.; O'Brien, M. C.; Husson, R. N.; B., D.; Kojima, E.; Broder, S.; Mitsuya, H. Changes in drug sensitivity of human immunodeficiency virus type 1 during therapy with azidothymidine, dideoxycytidine, and dideoxyinosine: An in vitro comparative study. *Proc. Natl. Acad. Sci. U.S.A.* **1993**, *90*, 562–566. (b) Perno, C. F.; Yarchoan, R.; Cooney, D. A.; Hartman, N. R.; Webb, D. S. A.; Hao, Z.; Mitsuya, H.; Johns, D. G.; Broder, S. Replication of HIV in monocytes: Granulocyte-macrophage colony stimulating factor (GM-CSF) potentiates viral production yet enhances the antiviral effect mediated by AZT and other dideoxynucleoside congeners of thymidine. *J. Exp. Med.* **1989**, *169*, 933–951.

JM8004543

doi:10.1016/j.jmb.2008.06.041 J. Mol. Biol. (2008) 381, 956–974

JMB

Available online at www.sciencedirect.com

ScienceDirect

ELSEVIER

Involvement of the Second Extracellular Loop and Transmembrane Residues of CCR5 in Inhibitor Binding and HIV-1 Fusion: Insights into the Mechanism of Allosteric Inhibition

Kenji Maeda[1], Debananda Das[1], Philip D. Yin[1], Kiyoto Tsuchiya[1], Hiromi Ogata-Aoki[2], Hirotomo Nakata[1], Rachael B. Norman[1], Lauren A. Hackney[1], Yoshikazu Takaoka[3] and Hiroaki Mitsuya[1,2]*

[1]*Experimental Retrovirology Section, HIV and AIDS Malignancy Branch, National Cancer Institute, National Institutes of Health, Bethesda, MD, USA*

[2]*Departments of Hematology and Infectious Diseases, Kumamoto University Graduate School of Medical and Pharmaceutical Sciences, Kumamoto, Japan*

[3]*Minase Research Institute, Ono Pharmaceutical Co. Ltd., Osaka, Japan*

Received 6 March 2008; received in revised form 12 June 2008; accepted 13 June 2008
Available online 20 June 2008

C-C chemokine receptor 5 (CCR5), a member of G-protein-coupled receptors, serves as a coreceptor for human immunodeficiency virus type 1 (HIV-1). In the present study, we examined the interactions between CCR5 and novel CCR5 inhibitors containing the spirodiketopiperazine scaffolds AK530 and AK317, both of which were lodged in the hydrophobic cavity located between the upper transmembrane domain and the second extracellular loop (ECL2) of CCR5. Although substantial differences existed between the two inhibitors—AK530 had 10-fold-greater CCR5-binding affinity (K_d = 1.4 nM) than AK317 (16.7 nM)—their antiviral potencies were virtually identical (IC_{50} = 2.1 nM and 1.5 nM, respectively). Molecular dynamics simulations for unbound CCR5 showed hydrogen bond interactions among transmembrane residues Y108, E283, and Y251, which were crucial for HIV-1-gp120/sCD4 complex binding and HIV-1 fusion. Indeed, AK530 and AK317, when bound to CCR5, disrupted these interhelix hydrogen bond interactions, a salient molecular mechanism enabling allosteric inhibition. Mutagenesis and structural analysis showed that ECL2 consists of a part of the hydrophobic cavity for both inhibitors, although AK317 is more tightly engaged with ECL2 than AK530, explaining their similar anti-HIV-1 potencies despite the difference in K_d values. We also found that amino acid residues in the β-hairpin structural motif of ECL2 are critical for HIV-1-elicited fusion and binding of the spirodiketopiperazine-based inhibitors to CCR5. The direct ECL2-engaging property of the inhibitors likely produces an ECL2 conformation, which HIV-1 gp120 cannot bind to, but also prohibits HIV-1 from utilizing the "inhibitor-bound" CCR5 for cellular entry—a mechanism of HIV-1's resistance to CCR5 inhibitors. The data should not only help delineate the dynamics of CCR5 following inhibitor binding but also aid in designing CCR5 inhibitors that are more potent against HIV-1 and prevent or delay the emergence of resistant HIV-1 variants.

Keywords: HIV-1; CCR5 inhibitor; GPCR structure; allosteric inhibition; extracellular loop

Edited by M. F. Summers

**Corresponding author.* E-mail address: hmitsuya@helix.nih.gov.

Abbreviations used: CCR5, C-C chemokine receptor 5; HIV-1, human immunodeficiency virus type 1; ECL2, second extracellular loop; GPCR, G-protein-coupled seven-transmembrane segment receptor; MVC, maraviroc; APL, aplaviroc; SDP, spirodiketopiperazine; TM1, transmembrane region 1; TM2, transmembrane region 2; TM3, transmembrane region 3; TM4, transmembrane region 4; TM5, transmembrane region 5; TM6, transmembrane region 6; TM7, transmembrane region 7; PHA, phytohemagglutinin; PBM, peripheral blood mononuclear; CHO, Chinese hamster ovary; mAb, monoclonal antibody; FCS, fetal calf serum; PDB, Protein Data Bank.

0022-2836/$ - see front matter. Published by Elsevier Ltd.

Introduction

C-C chemokine receptor 5 (CCR5) is a member of G-protein-coupled seven-transmembrane segment receptors (GPCRs), which comprise the largest superfamily of proteins in the body.[1] In 1996, it was revealed that CCR5 represents one of the two essential coreceptors for human immunodeficiency virus type 1 (HIV-1) entry into human $CD4^+$ cells, thereby serving as an attractive target for possible intervention for HIV-1 infection using CCR5 as a coreceptor (R5-HIV-1).[2–5] The second extracellular loop (ECL2) of GPCRs is known to play a critical role in ligand binding and ensuing signal transduction. The ECL2 of CCR5 is also thought to play an important role in CCR5 interactions with HIV-1 envelope. To date, scores of newly designed and synthesized CCR5 inhibitors have been reported to be potent against R5-HIV-1;[6–15] one such inhibitor, maraviroc (MVC),[11,15] has recently been approved by the US Food and Drug Administration for treatment of HIV-1-infected individuals who do not respond to any existing antiretroviral regimen.

HIV-1 gp120 interacts with CCR5 following its binding to CD4, and such an interaction is thought to involve the V3 region of gp120 and the N-terminus and extracellular loops of CCR5.[16,17] Recent reports[18–21] have determined the orientation and location of CCR5 inhibitors within CCR5 and have shown that those inhibitors are all located in a hydrophobic cavity formed by the transmembrane domains of CCR5. In fact, earlier reports demonstrated that mutations in the extracellular loops did not have any effect on the binding of CCR5 inhibitors SCH-C and TAK-779.[19,22,23] Taking these observations together, the binding sites in CCR5 for CCR5 inhibitors distinctly differ from the binding sites in CCR5 for HIV-1 gp120, strongly suggesting that CCR5 inhibitors block the interactions of CCR5 with HIV-1 gp120 by eliciting allosteric changes in extracellular loop structures.[9,22,23]

We previously reported a small-molecule CCR5 inhibitor, aplaviroc (APL; 4-[4-[(3*R*)-1-butyl-3-[(1*R*) cyclohexylhydroxymethyl]-2,5-dioxo-1,4,9-triazaspiro [5.5] undec-9 ylmethyl] phenoxy] benzoic acid hydrochloride), which has a high affinity for CCR5 (K_d values of 3 nM) and exerts potent activity against a wide spectrum of R5-HIV-1 isolates, including multidrug-resistant R5-HIV-1 strains.[14,24] APL significantly reduced viremia in patients with HIV-1 infection, as examined in a phase 2a clinical trial in the United States. However, in phase 2b clinical trials enrolling about 300 patients, four individuals receiving APL developed grade 3 or greater treatment-emergent elevations in ALT; in late 2005, the clinical development of APL was terminated. However, using APL as a specific probe, we further conducted structural analyses of CCR5 inhibitor interactions with CCR5, employing homology modeling, robust structure refinement, and molecular docking based on site-directed-mutagenesis-based saturation binding assay data of CCR5 inhibitors.[22]

In the current study, we determined the structural and molecular interactions of two novel CCR5 inhibitors, AK530 [(3*S*)-1-but-2-yn-1-yl-3-[(1*S*)-cyclohexyl-hydroxymethyl]-9 (3,5-dimethyl-1-phenyl-1*H*-pyrazol-4-ylmethyl)-1,4,9-triazaspiro [5.5] undecane 2,5-dione dihydrochloride] and AK317 [4-(4-{[(3*S*)-1-butyl-3-(cyclohexylmethyl)-2,5-dioxo-1,4,9-triazaspiro[5.5] undec-9-yl] methyl} phenoxy) benzoic acid hydrochloride] (Fig. 1), both of which contain a novel spirodiketopiperazine (SDP) scaffold. We found that these two inhibitors lodge in a hydrophobic cavity located between the upper transmembrane domain and the ECL2 of CCR5. We found substantial differences between the two molecules: AK530 had a 10-fold-greater CCR5-binding affinity (K_d = 1.4 nM) than AK317 (K_d = 16.7 nM), while their antiviral potencies were virtually identical [IC_{50} = 2.1 nM (AK530) and 1.5 nM (AK317)]. Modeling analysis showed that AK530 has the least interactions with S180 and K191 of ECL2, with which AK317 has a close association, suggesting that the interaction profile of the inhibitors with ECL2 residues is one of the important determinants of antiviral potency. We also found that the hairpin motif in the N-terminal half of ECL2 is critical for HIV-1-envelope-elicited fusion event. The direct ECL2-engaging property of the inhibitors likely produces an ECL2 conformation, which HIV-1 gp120 cannot bind to, but also prohibits or substantially delays the emergence of HIV-1 that utilizes the "inhibitor-bound" CCR5 for cellular entry—a mechanism of HIV-1's resistance to CCR5 inhibitors. We also carried out molecular dynamics simulations of unbound CCR5 and compared the conformation with inhibitor-bound CCR5. Critical interhelix hydrogen bond interactions and interactions between the helices and the ECL2 seen in the unbound CCR5 were lost when transmembrane helix residues rearranged to

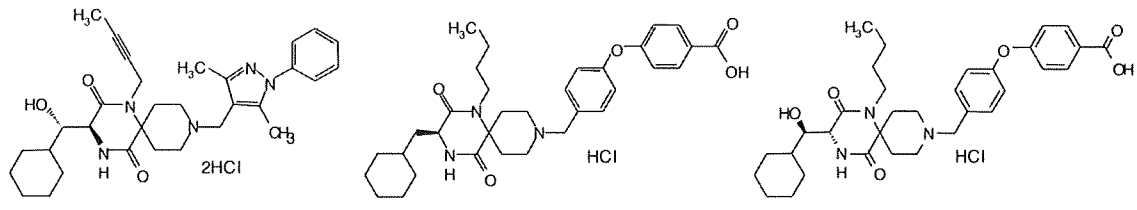

Fig. 1. Structures of small-molecule CCR5 inhibitors AK530, AK317, and APL.

accommodate AK530 and AK317 in the binding pocket. These observations add considerable insights into the mechanism of the allosteric inhibition of CCR5–gp120 interaction by CCR5 inhibitors.

Results

Structural modeling of unliganded human CCR5

It is thought that the ECL2 of human CCR5 (Fig. 2) plays an important role in the binding of CC chemokines to CCR5, as well as in the binding of HIV-1-gp120/CD4 complex to CCR5 in the cellular entry of HIV-1.[25,26] On the other hand, certain amino acid residue substitutions such as Y108A, Y251A, and E283A, all of which are located in the transmembrane domain (Fig. 2a), significantly reduce both HIV-1-gp120/CD4 complex binding to CCR5 and HIV-1 susceptibility of CCR5-expressing cells, as previously described.[22]

In the present study, in an attempt to examine the interplays of ECL2 and selected amino acid residues consisting of the largest hydrophobic cavity within CCR5, which accommodates small-molecule CCR5 inhibitors, we generated a homology model of CCR5, without any ligands bound, using the crystal structure of bovine rhodopsin as template.[27] In generating the model, the following structural assignment to CCR5 was made: residues 1 through 26 were assigned to the N-terminus region; residues 27 through 57 were assigned to transmembrane region 1 (TM1); residues 58 through 63 were assigned to the first cytoplasmic region; residues 64 through 93 were assigned to transmembrane region 2 (TM2); residues 94 through 96 were assigned to the first extracellular loop; residues 97 through 130 were assigned to transmembrane region 3 (TM3); residues 131 through 141 were assigned to the second cytoplasmic region; residues 142 through 165 were assigned to transmembrane region 4 (TM4); residues 166 through 190 were assigned to ECL2; residues 191 through 219 were assigned to transmembrane region 5 (TM5); residues 220 through 231 were assigned to the third cytoplasmic region; residues 232 through 259 were assigned to transmembrane region 6 (TM6); residues 260 through 278 were assigned to the third extracellular loop; residues 279 through 300 were assigned to transmembrane region 7 (TM7); residues 303 through 312 were assigned to the helix region (H8) in the cytoplasmic domain; and residues from 313 were assigned to the C-terminus (Fig. 2).

To more effectively sample the conformational space occupied by CCR5, we carried out molecular dynamics simulation for 4800 ps to efficiently explore the conformational space of CCR5. The simulation was carried out in implicit water with a time step of 1 fs, and without any distance cutoffs for nonbonded van der Waals and electrostatic interactions. These stringent conditions added considerably to the overall computation time, but are thought to provide robust results. The conformations at intervals of 50 ps were analyzed. As expected, there are several hydrogen bonds between nearby residues in the same transmembrane helix that are important for maintaining the helical structure. Examples of such interactions are between W248 and Y251 in TM6, and between E283 and M287 in TM7 (Fig. 3).

We identified a hydrogen bond network involving multiple helices and ECL2: Y108(TM3), E283(TM7), Y251(TM6), and S180(ECL2) (Fig. 3). These hydrogen bond interactions were considered particularly important for the following reason. Interhelical hydrogen bonds have been shown to be critical in maintaining inactive conformations of G-protein-coupled receptors.[28] For rhodopsin, whose structure–function relationships have been studied widely using biochemical and spectroscopic methods, movement of TM3 and TM6 helices is known to produce changes in loop conformations.[29] This interhelix movement takes place due to the loss of hydrogen bond interactions between TM3 and TM6 residues. The loss of hydrogen bond network between transmembrane helices, mediated through water molecules, has also been thought to be responsible for carrying out changes in the loop conformations with functional implications.[30] When AK530 and AK317 were bound to CCR5, Y108 rotated away from Y251, and the hydrogen bonds between Y108 and E283 and between E283 and S180 were lost (see below). The change in this polar interaction might be responsible for changes in CCR5 loop conformation inhibiting gp120 interaction.

Activity against R5-HIV-1 and the CCR5-binding affinity of CCR5 inhibitors

We determined the activity of two novel SDP-based CCR5 inhibitors, AK530 and AK317 (Fig. 1), against R5-HIV-1 on a cell-based acute R5-HIV-1 exposure assay using the HeLa-CD4-LTR-β-gal indicator cell line expressing human CCR5 [$CD4^+$,$CCR5^+$ MAGI cells] and phytohemagglutinin (PHA) peripheral blood mononuclear (PBM) cells as target cells with two different R5-HIV-1 species, HIV-1_{JRFL} and HIV-$1_{Ba\text{-}L}$. We also conducted a saturation binding assay using ^{3}H-labeled AK530 and AK317 and $CCR5_{WT}$-expressing Chinese hamster ovary (CHO) cells, and determined their binding affinity for $CCR5_{WT}$ (K_d; dissociation constant values), as previously described.[14] As shown in Table 1, AK530 exerted potent antiviral activity against both HIV-1_{JRFL} and HIV-$1_{Ba\text{-}L}$ in two different target cells, with IC_{50} values ranging from 2.1 nM to 32 nM, and proved to have a high binding affinity for CCR5, with a K_d value of 1.4± 0.9 nM. AK317 was comparably potent against the virus (IC_{50}=1.5–25 nM), but had a lower CCR5-binding affinity than AK530 by about a factor of 10 (K_d=16.7±7.5 nM). Neither of these CCR5 inhibitors had activity against X4-HIV-1 (data not shown). For comparison, the antiviral potency and binding affinity of APL[14] are illustrated in Table 1. APL had greater anti-HIV-1 activity (IC_{50}=0.2–0.7 nM) than AK530 and AK317, but its binding affinity (K_d=3.6± 1.3 nM) was slightly less than that of AK530.

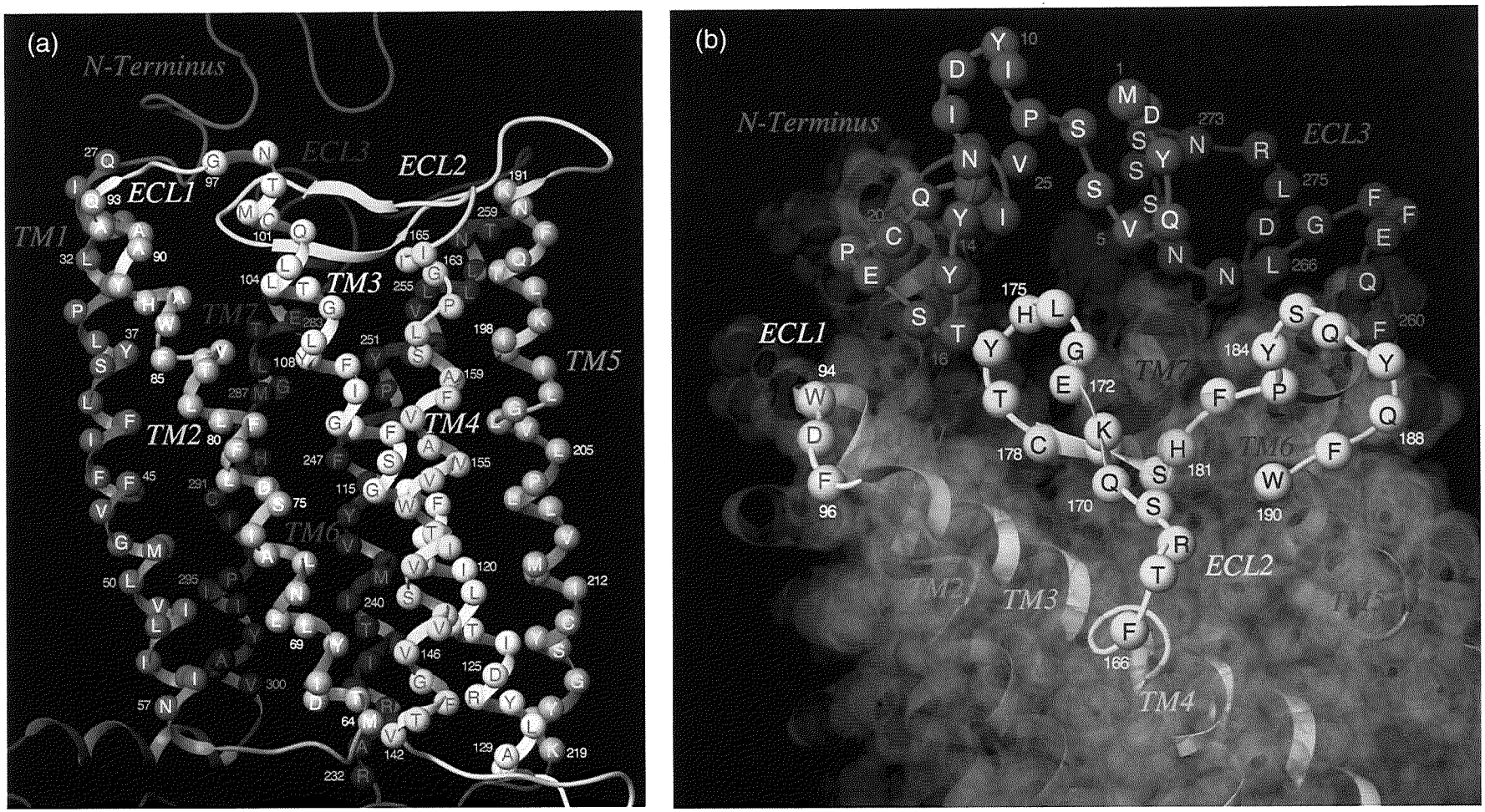

Fig. 2. The transmembrane helices and extracellular loop regions of CCR5. (a) A side view of the transmembrane domains. TM2, TM3, and TM4 are above the plane of the paper, and TM6 and TM7 are below the plane. The following assignments have been made for transmembrane helices: TM1, residues 27–57; TM2, residues 64–93; TM3, residues 97–130; TM4, residues 142–165; TM5, residues 191–219; TM6, residues 232–259; TM7, residues 279–300. (b) A top view of the extracellular loop regions. The following assignments have been made for loops: N-terminus, residues 1–26; first extracellular loop, residues 94–96; ECL2, residues 166–190; third extracellular loop, residues 260–278.

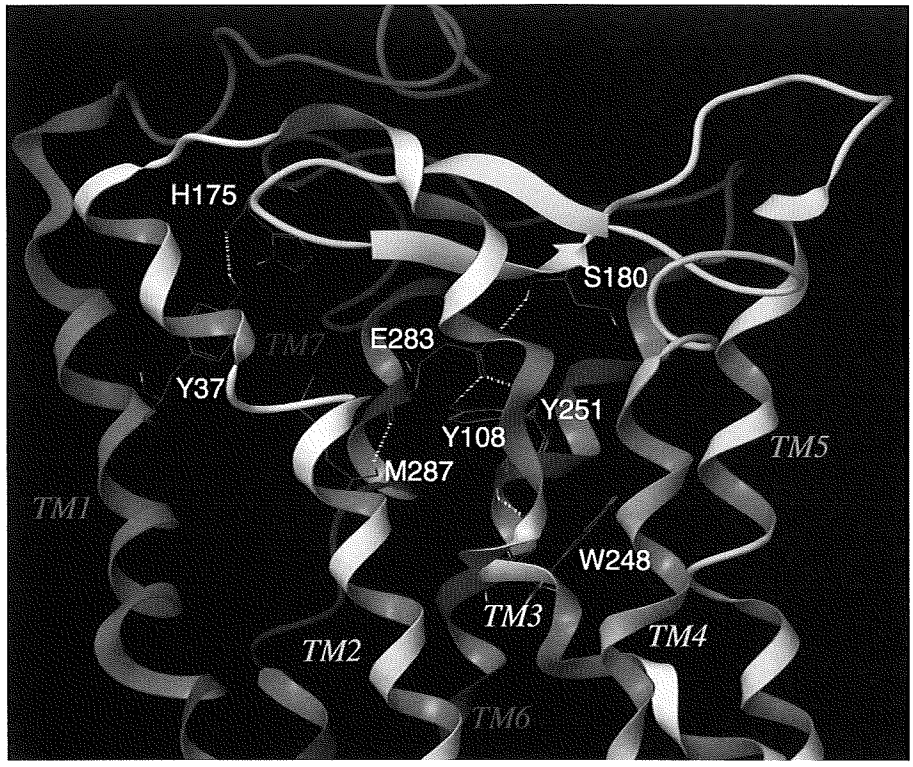

Fig. 3. Transmembrane residues Y108(TM3)/E283(TM7)/Y251(TM6)/M287(TM7)/S180(ECL2) of unliganded CCR5, forming a hydrogen bond network. Y37 has a hydrogen bond interaction with H175. This shows that transmembrane residues, which have been implicated in CCR5 inhibitor binding, have direct interactions with ECL2 residues in the unliganded receptor. It is assumed that these intramolecular interactions are responsible for maintaining a conformation of ECL2 that is favorable for binding with the HIV-1-gp120/CD4 complex. AK530 interacts with Y37, Y108, E283, and Y251 in the binding cavity and disrupts the intramolecular interactions of Y108 and Y251 with E283, and those of E283 with the ECL2 (Fig. 5). It is assumed that these structural changes, after inhibitor binding, alter the conformation of the ECL2, resulting in loss of association with gp120. The analysis strongly suggests that the loss of hydrogen bonds between helices may cause allosteric conformational changes in ECL2, leading to the inhibition of HIV-1 gp120 binding to CCR5.

Profiles of the binding affinity of [^{3}H]AK530 and [^{3}H]AK317 for a panel of mutant CCR5-expressing cells

In order to explain the difference in the anti-HIV-1 activity and CCR5-binding profiles described above, we determined the binding affinity of [^{3}H]AK530 and [^{3}H]AK317 by employing a panel of mutant CCR5-overexpressing CHO cells. As shown in Table 2, we found that the K_d values of AK530 drastically increased, as examined in CHO cells expressing such CCR5 mutations as Y37A, C101A, F109A, G163R, C178A, T195P, T195S, and Y251A, with all K_d values being >100 nM (>71-fold greater than that with $CCR5_{WT}$). AK317, whose affinity for wild-type CCR5 was nearly 10-fold lower than AK530, also had a significant decrease in its binding affinity with these mutations, with all K_d values being >100 nM (>5.9-fold greater than that with $CCR5_{WT}$). As for G163, a Gly-to-Arg substitution was examined in this study because the G163R substitution has been reported to reduce susceptibility to HIV.[31] In addition, AK317 had a significantly decreased binding affinity for CCR5 when it contained P84H, Y108A, K191A/N, I198A,

Table 1. Anti-HIV activity against WT-R5-HIV-1 and binding affinity for WT-CCR5 of CCR5 inhibitors

Compound		Antiviral assay (virus) [nM]			Binding assay (K_d) [nM]
		MAGI with HIV-1_{JRFL}	MAGI with HIV-1_{Ba-L}	PHA-PBM with HIV-1_{Ba-L}	
AK530	IC_{50}[a]	2.8±1.5[b]	2.1±1.1	32±27	1.4±0.9
	IC_{90}	51±2.5	79±34	430±113	
AK317	IC_{50}	2.0±0.2	1.5±1.9	25±8	16.7±7.5
	IC_{90}	19±14	25±3	171±45	
APL	IC_{50}	0.2±0.1	0.2±0.1	0.7±0.4	3.6±1.4
	IC_{90}	1.8±0.7	2.9±1.6	12±10	

[a] IC_{50} values were determined with the MAGI assay and the PHA-PBM (p24) assay (see Materials and Methods).
[b] The numbers denote the IC_{50}, IC_{90}, or K_d values (mean±SD).

Table 2. Binding affinity of CCR5 inhibitors for mutant CCR5

Mutant CCR5 in CHO cells		K_d value [nM]		
		AK530	AK317	APL
Wild type		1.4±0.9	16.7±7.5	3.6±1.4
D11A	*NH_2 terminus*	1.1±0.5	14.6±1.9	3.0±0.6[a]
Y37A	*TM1*	**>100**	**>100**[b]	12.8±0.9
P84H	*TM2*	**37.3±6.3**	**>100**	**>100**
C101A	*TM3*	**>100**	**>100**	**>100**
L104D	*TM3*	6.8±0.7	**93.3±26.4**	**18.3±3.6**
Y108A	*TM3*	**60.7±26.2**	**>100**	**19.8±4.4**[a]
F109A	*TM3*	**>100**	**>100**	**>100**
F112L	*TM3*	5.4±2.1	14.7±2.5	4.0±2.6[a]
F112Y	*TM3*	5.2±3.4	21.1±8.9	6.8±1.1[a]
F113A	*TM3*	2.4±0.3	43.3±7.4	13.3±2.3[a]
F113Y	*TM3*	2.8±0.5	48.2±10.2	12.9±3.1
G163A	*TM4*	5.9±2.6	14.7±0.1	8.0±4.2[a]
G163R	*TM4*	**>100**	**>100**	**>200**[a]
R168A	*ECL2*	2.2±0.7	24.6±4.1	14.1±9.4
K171A/E172A	*ECL2*	3.5±1.2	14.7±0.1	2.8±0.1[a]
C178A	*ECL2*	**>100**	**>100**	**>200**[a]
S180A	*ECL2*	**7.4±1.4**	34.5±7.9	5.7±1.2[a]
S180T	*ECL2*	1.4±0.6	14.9±1.7	1.5±0.6[a]
S180E	*ECL2*	5.7±2.3	61.8±22.9	13.9±1.7[a]
Y184A/S185A	*ECL2*	2.2±2.3	14.8±0.2	2.0±0.8[a]
Y184A/S185A/ Q186A/Y187A	*ECL2*	2.2±0.4	22.0±4.2	2.0±0.6[a]
Q186A/Y187A	*ECL2*	2.3±0.1	14.4±2.2	2.8±0.5[a]
Q188A	*ECL2*	1.9±1.3	14.6±3.6	6.6±1.4[a]
K191A	*ECL2-TM5*	6.0±3.8	**>100**	**>200**[a]
K191R	*ECL2-TM5*	5.2±2.8	22.2±7.7	9.0±5.6[a]
K191N	*ECL2-TM5*	**12.5±3.3**	**>100**	14.2±1.1[a]
T195A	*TM5*	5.6±3.9	14.7±0.1	**48.1±4.3**
T195P	*TM5*	**>100**	**>100**	**>100**
T195S	*TM5*	**>100**	**>100**	**>100**
K197A	*TM5*	**7.6±3.7**	58.3±18.7	10.7±3.5
I198A	*TM5*	**9.8±2.2**	**>100**	**24.6±4.8**[a]
W248A	*TM6*	**43.4±4.5**	**>100**	**29.8±4.6**
Y251A	*TM6*	**>100**	**>100**	**36.5±9.5**[a]
E283A	*TM7*	**19.1±2.5**	**>100**	**>200**[a]
M287A	*TM7*	2.4±1.4	16.1±2.1	6.8±2.3[a]
M287E	*TM7*	**62.7±17.8**	**87.1±0.6**	14.8±1.7[a]

[a] Data from Maeda *et al.*[22]
[b] K_d values more than fivefold that of $CCR5_{WT}$ are shown in boldface.

W248A, or E283A (all K_d values >100 nM). It was seen that APL significantly decreased its binding affinity (K_d values of >100 nM, >27-fold lower than that with $CCR5_{WT}$) for CCR5 when it contained a P84H, C101A, F109A, G163R, C178A, K191A, T195P/S, or E283A substitution. Thus, AK317, whose CCR5-binding affinity for $CCR5_{WT}$ was >4-fold lower than that of APL, had virtually the same binding profile as that of APL, while two additional mutations (Y108A, and Y251A), which decreased the CCR5-binding affinity of APL (K_d values <100 nM), also nullified the CCR5 binding of AK317, consistent with the notion that the affinity of AK317 for $CCR5_{WT}$ is lower than that of APL. It was noted that as the K191A substitution significantly reduced the CCR5-binding affinity of both AK317 and APL, it had moderately (4.2-fold) reduced the binding affinity of AK530. Moreover, the Y37A substitution, which caused only a <4-fold reduction in the CCR5 binding of APL (Table 2), produced a significant reduction in the CCR5 binding of AK530 and AK317. Other dissociations in the K_d profiles between APL and AK530 were seen when CCR5 had an amino acid substitution at Y108A (5.5-fold for APL *versus* 43.3-fold for AK530), Y251A (10.1-fold for APL *versus* >71-fold for AK530), or E283A (>55-fold for APL *versus* 13.6-fold for AK530). Taken together, the results obtained with the saturation binding assay using the ^{3}H-labeled CCR5 inhibitors employed here suggest that the binding profile of AK317 is similar to that of APL; the binding profiles of AK530 and APL share some common features and possibly have some important differences, while both AK530 and AK317 are comparably potent against R5-HIV-1.

Amino acid residues of CCR5 crucial for the interactions with CCR5 inhibitors

We subsequently defined a three-dimensional model of human CCR5–CCR5 inhibitor complex by combining the results of the site-directed-mutagenesis-based analyses described above (Table 2) and molecular modeling that involved structural refinement and docking of inhibitors to an initial structure of CCR5 based on the crystal structure of bovine rhodopsin.[30,32]

Of note, both amino acid substitutions C101A (TM3) and C178A(ECL2) virtually nullified the binding of all three CCR5 inhibitors examined: AK530, AK317, and APL (Table 2). These findings confirmed the assumption that C101 and C178 form a disulfide bond that is crucial in maintaining the conformation of the ECL2. These data also strongly suggest that either of the two amino acid substitutions disrupted the disulfide link, altered the conformation of the loop, and nullified the binding of the three CCR5 inhibitors to CCR5. This binding profile common to AK530, AK317, and APL indicates that their binding to CCR5 is sensitive to the ECL2 conformation and significantly differs from the binding profile of other CCR5 inhibitors such as SCH-C and TAK-779, which do not undergo drastic loss in their CCR5 binding with these mutations.[19,22,23]

The model of CCR5 complexed with a CCR5 inhibitor that we generated in the present study was derived by taking the flexibility of both CCR5 and the inhibitor into account and by computationally designating a model that most suitably provided a rational explanation of the mutagenesis data. In the present study, we chose a few CCR5 residues, which were predicted to have significant interactions with the inhibitor based on our initial model.[22] The residues chosen for mutation were P84, L104, F109, T195, and W248. P84 was observed to be in close contact with APL in these models (Fig. 4c), and CCR5 containing a P84H substitution ($CCR5_{P84H}$) was generated. The binding affinity of APL for $CCR5_{P84H}$ decreased by nearly 30 times compared to wild-type CCR5 ($CCR5_{WT}$) and confirmed that the binding of APL is indeed dependent on this residue (Table 2). L104 was

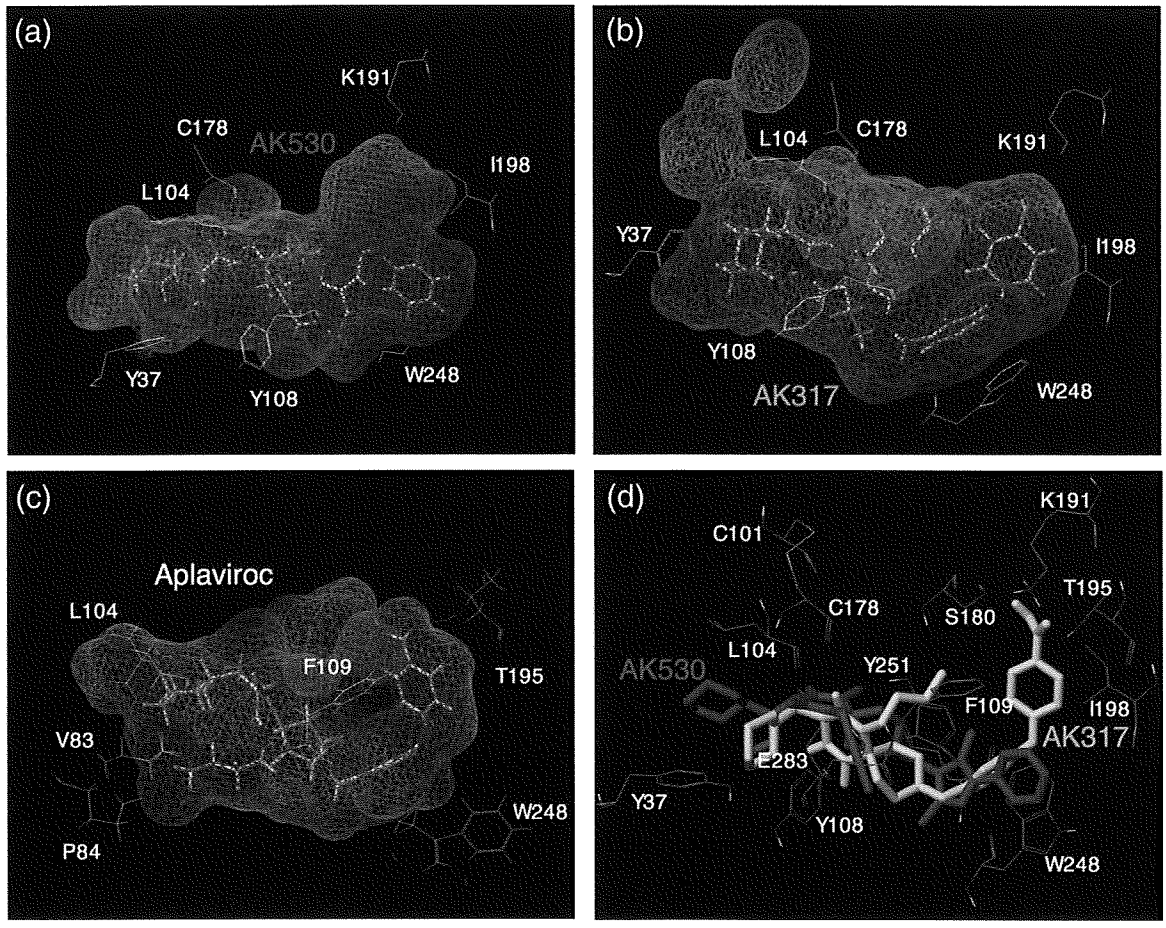

Fig. 4. Lipophilic potential mapped on the binding cavity of CCR5 inhibitors. The lipophilic potential mapped onto the binding cavity when AK530, AK317, and APL bind to CCR5 are shown in (a), (b), and (c), respectively. The predominantly lipophilic region of the cavity is shown in brown (bottom region of the cavity, which is located towards the cytoplasmic region of CCR5). The blue regions are predominantly hydrophilic (present towards the extracellular region), and the green regions are moderately lipophilic. The figure was generated using MOLCAD. The shapes of the binding cavity are slightly different for AK530 and AK317, as receptor conformations are slightly different when these molecules bind to CCR5. The unoccupied volumes of the cavities suggest optimization ideas for improving the potency of these molecules. (d) The binding modes of AK530 and AK317 superimposed. AK530 is shown in red, and AK317 is shown in green. Note that the binding orientations in the vicinity of transmembrane helices 5 and 6 differ. AK317 binds towards and around ECL2 residues, whereas AK530 bends towards the intracellular domain. AK530 has a high binding affinity probably because it binds "deeper" into the cavity. On the other hand, by being able to interact with ECL2 residues, AK317 maintains comparable anti-HIV-1 potency with AK530 even though its binding affinity is about 10-fold lower.

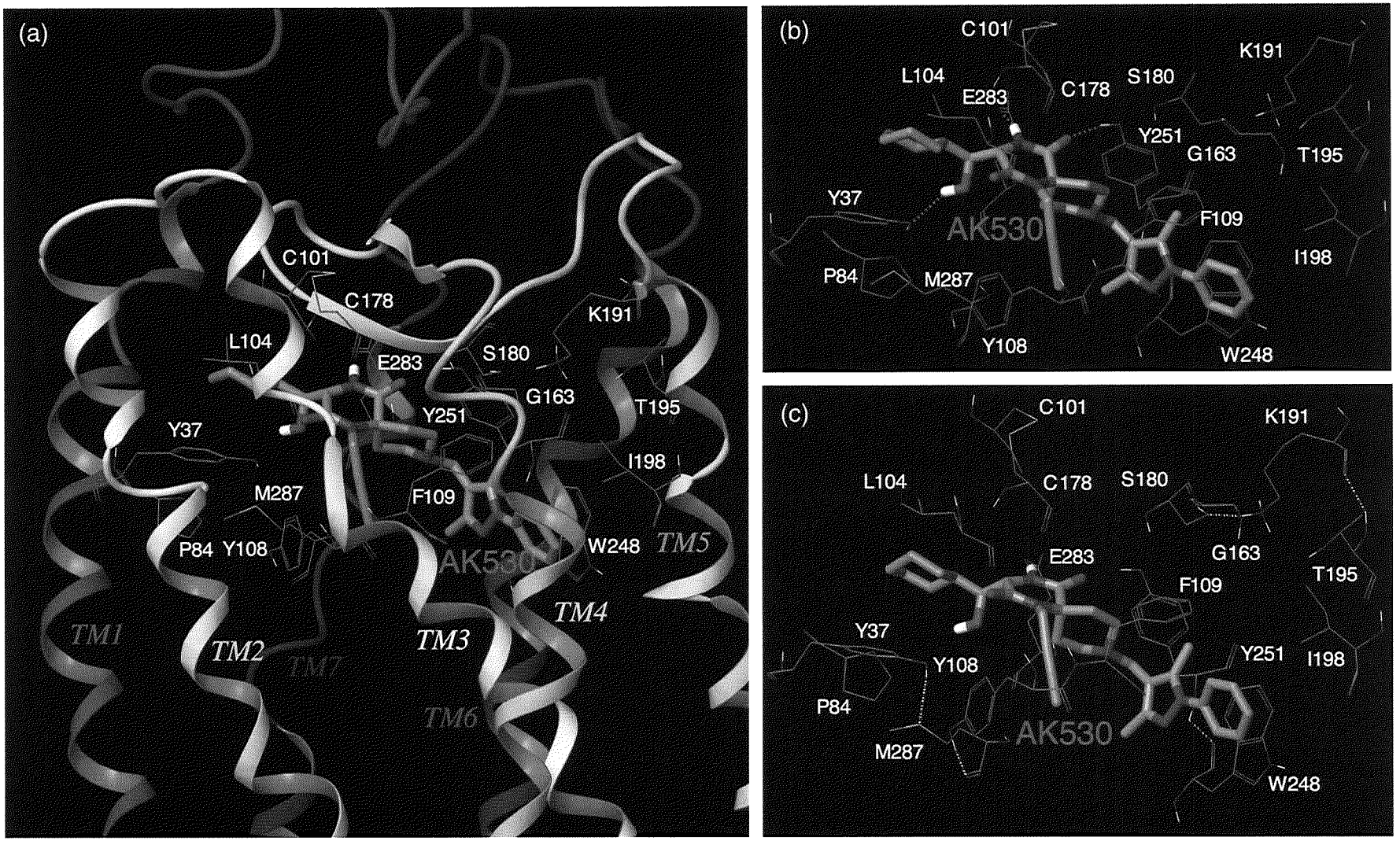

Fig. 5. Amino acid residues forming the binding cavity within CCR5 for AK530. (a) The amino acid residues forming the binding cavity of CCR5 and the binding mode of AK530 are shown. The transmembrane regions and the ECL2 enclose the cavity. Every transmembrane helix has at least one residue that contributes towards forming the binding pocket for AK530. (b) AK530 is predicted to have hydrogen bond interactions with Y37(TM1), Y251(TM6), and E283(TM7), and has favorable hydrophobic interactions with several binding site residues, including P84, L104, F109, and I198. The benzene ring of AK530 forms a π–π interaction with W248. (c) The hydrogen bond networks, involving multiple transmembrane domains, define the shape of the CCR5 cavity for AK530. There is one network of hydrogen bonds involving Y37(TM1), M287(TM7), and Y108(TM3). Another network involves S180(ECL2), G163(TM4), K191(TM5), and T195(TM5). The hydrogen bond networks are different for the unbound and inhibitor-bound CCR5.

also in the proximity of APL-binding cavity (Fig. 4c), and $CCR5_{L104D}$ was generated, proving a decrease in the binding affinity of APL by about fivefold (Table 2). The binding affinities of SCH-C and TAK-779 for $CCR5_{P84H}$ and $CCR5_{L104D}$ were also determined, and there were minimal changes from the wild-type binding affinity (K_d changed by only twofold to threefold). This indicates that P84 and L104 are likely in close contact with APL, and the decrease in the binding affinity of $CCR5_{P84H}$ and $CCR5_{L104D}$ mutants is not predominantly due to any drastic conformational changes that might have accompanied these mutations. The models examined in this study showed that F109 forms a $\pi-\pi$ interaction with APL (Fig. 4c). F109 is present in a cluster of aromatic residues involving other nearby phenylalanine and tyrosine residues in the binding pocket. $CCR5_{F109A}$ was generated, proving a drastic loss of APL, AK317, and AK530 binding to CCR5 (Table 2). SCH-C and TAK-779 also had K_d values higher than 100 nM, indicating that F109 is important for the binding of structurally diverse CCR5 inhibitors. T195 was chosen because it was observed that the inhibitors were shown to have different dependences on their binding affinity for this residue. The model for APL (Fig. 4c) showed that an intramolecular hydrogen bond network involving S180/G163/K191/T195 is important for defining the binding cavity for APL, and APL *per se* also has a potential hydrogen bond interaction with T195 (Fig. 4c). The intramolecular hydrogen bond network of CCR5 was not observed in our models of CCR5 complexed with SCH-C or TAK-779. Moreover, SCH-C or TAK-779 does not have any groups or atoms capable of forming hydrogen bond interactions with T195. Indeed, the K_d values for APL for $CCR5_{T195P}$ and $CCR5_{T195S}$ were >100 nM (Table 2), while the binding profile of SCH-C and TAK-779 to CCR5 was not affected by T195P or T195S substitutions [K_d values of SCH-C: 16.0 nM (wild type), 28.9 nM (T195P), and 21.7 nM (T195S); K_d values of TAK-779: 30.2 nM (wild type), 31.1 nM (T195P), and 32.5 nM (T195S)]. Interestingly, in CCR5 complexed with AK530 and AK317, the hydrogen bond network with S180, G163, K191, and T195 was seen, suggesting that the network led to maintain a conformation of CCR5 suitable for the binding of SDP-based inhibitors. Indeed, both AK530 and AK317 failed to bind to $CCR5_{T195P}$ and $CCR5_{T195S}$, although AK530 did not have a direct interaction with the network (Fig. 5). Taken together, these results sustained our notion that the CCR5 inhibitor–CCR5 interactions generated based on the rhodopsin crystallographic data are reasonably reliable.

Structural analysis of AK530 and AK317 interactions with CCR5

The structural interactions of AK530 with CCR5 are shown in Fig. 5a–c. The binding cavity of AK530 involves residues from each of the transmembrane domains and the ECL2. The binding cavity is stabilized by several intramolecular hydrogen bonds involving residues in different transmembrane regions. Y37, M287, and Y108, which are in transmembrane helices 1, 7, and 3, respectively, form a hydrogen bond network that defines one end of the cavity. Another network involves S180(ECL2), G163(TM4), K191 (TM5), and T195(TM5). AK530 binds in a somewhat diagonal fashion, reaching deeper into the cavity of CCR5, and has several polar and nonpolar interactions that give rise to its very high affinity (K_d = 1.4 nM). The hydroxymethylene of AK530 is predicted to have a hydrogen bond interaction with the side chain of Y37, and the diketopiperazine ring of AK530 is predicted to have a hydrogen bond interaction with the side chains of Y251 and E283. The hydrophobic interactions that stabilize binding involve P84, L104, and I198. There are $\pi-\pi$ interactions involving F109 and W248. Indeed, the binding affinity of CCR5 species containing Y37A, Y108A, or W248A was drastically reduced in our saturation binding assays, and the residues implicated in the binding of AK530 as described above appear to have an important structural significance. F109 is present in a cluster of aromatic residues in TM3. W248 is part of a highly conserved set of residues present in the TM6 of class A GPCRs. E283 is the fifth residue in TM7. This position has been shown to be involved in the binding of small-molecule ligands to several chemokine receptors.[33] It is noteworthy that we have demonstrated that the E283 residue is important not only in the binding of other CCR5 ligands such as SCH-C and TAK-779 but also in preserving the C-C chemokine/CCR5 interactions and HIV-1-gp120/CD4 complex binding to CCR5.[22]

The binding site residues and the binding mode of AK317 are shown in Fig. 6a and b. AK530 and AK317 are analogues and are expected to share certain common features of CCR5 binding. However, important structural differences were identified between the two analogues. AK530 has a cyclohexyl-hydroxymethyl group, whereas AK317 only has a cyclohexyl-methyl group. AK530 has a phenyl-pyrazol moiety, while AK317 has a phenoxy-benzoic acid group as substituent. The carboxylate group of the benzoic acid in AK317 forms hydrogen bond interactions with S180, K191, and T195. These three residues, along with G163, are involved in an intra-CCR5 hydrogen bond network. Thus, it appears that K191 and T195 are not only important in defining the shape of the cavity but are also involved in directly binding with AK317. AK317 has van der Waals interactions with P84, Y108, I198, and Y251, and $\pi-\pi$ interactions with F109 and W248. Another intra-CCR5 hydrogen bond network involving Y37(TM1), E283(TM7), M287(TM7), and Y108(TM3) is responsible for defining the binding cavity. As shown in Fig. 4a and b, the size and shape of the binding cavity of AK530 appear to differ from those of AK317, and the superimposition of the binding modes of AK317 and AK530 clearly shows that although these two inhibitors share certain common binding features, the orientations and topography of these two inhibitors are substantially different (Fig. 4d).

As described above, in spite of sharing a common core, the different substituents make the conformation of these two molecules different, giving rise to differences in structural interactions with CCR5. The binding orientations differ the most around TM5 and